Scientific Research Publishing

Energy and Power Engineering, 2026, 18(6), 329-373
https://www.scirp.org/journal/epe
ISSN Online: 1947-3818
ISSN Print: 1949-243X

IRFO-Based Ride-Through Control of a Dual-Stator Induction Motor (MACU) under Voltage Unbalance: Modeling and Experimental Validation

Rodolphe Gomba, Ursula Vanelie Kani Mboyo, Tite Lawd Ngouloubi, Amos Omboua Eyandzi

Polytechnic Superior National School (ENSP), Marien Ngouabi University, Brazzaville, Congo
Email: ngouloubitite@gmail.com

How to cite this paper: Gomba, R., Kani Mboyo, U.V., Ngouloubi, T.L. and Omboua Eyandzi, A. (2026) IRFO-Based Ride-Through Control of a Dual-Stator Induction Motor (MACU) under Voltage Unbalance: Modeling and Experimental Validation. *Energy and Power Engineering*, **18**, 329-373.
https://doi.org/10.4236/epe.2026.186017

Received: March 28, 2026
Accepted: June 12, 2026
Published: June 15, 2026

Abstract

Voltage unbalance and phase loss are common disturbances in weakly interconnected power systems and significantly degrade the performance of induction motor drives. This paper proposes a fault-tolerant solution based on a Universal Cage Induction Motor (MACU) featuring a dual-stator architecture composed of a main three-phase winding and an auxiliary single-phase winding. This configuration introduces magnetic redundancy, enabling the preservation of rotor flux under severe unbalanced supply conditions. A comprehensive electromagnetic model of the MACU is developed in the rotating (dq) reference frame, accounting for stator coupling, capacitor effects, and symmetrical component interactions under unbalance. An IRFO (*Indirect Rotor Field Orientation*)-based control strategy is implemented to regulate flux and torque, including an automatic ride-through mechanism enabling transition from three-phase to single-phase operation. Simulation and experimental validation on a dedicated test bench show that the proposed system maintains operation under high unbalance levels (up to $k_U \approx 80\%$), with rotor flux deviation below 3% and mechanical speed variation below 2.7% during transitions. The comparison between simulation and measurements indicates deviations below 3% for key variables. These results indicate that the MACU combined with IRFO control provides a fault-tolerant drive solution with reduced structural complexity compared to multiphase architectures, while maintaining stable operation under severe grid disturbances.

Keywords

Universal Cage Induction Motor (MACU), Dual-Stator Machine,

Ride-Through Control, Voltage Unbalance, IRFO Control, Fault-Tolerant Drive, Rotor Flux Orientation, Experimental Validation

1. Introduction

Squirrel-cage induction motors are currently the core component of most industrial drive systems. Their widespread adoption is explained by their robustness, relatively low cost, ease of maintenance, and long service life. More than 80% of modern electromechanical installations continue to rely on this technology, particularly in contexts where the power supply is unstable. In many weakly interconnected networks, voltage variations, micro-outages, overvoltages, and phase loss represent common disturbances that can compromise operational continuity. These issues are observed in various contexts, particularly in certain regions of Central Africa where voltage unbalances can become highly pronounced [1] [2].

Although robust, induction motors remain sensitive to electrical asymmetries. An unbalance introduces a negative-sequence component in the stator quantities, which generates a rotating field opposite to the main field. This interaction produces a torque oscillation at twice the grid frequency and leads to increased Joule losses, excessive winding heating, reduced efficiency, and mechanical vibrations that can accelerate wear. Even small unbalances, below 5%, can result in an increase of more than 20% in losses. When the asymmetry becomes significant, the control system struggles to stabilize flux and torque, potentially leading to loss of synchronism or complete shutdown of the machine [3]-[5].

Conventional control techniques provide a limited response to such conditions. Scalar control, although simple, fails to simultaneously ensure flux and torque stability when voltages become unbalanced. Direct Torque Control (DTC), known for its fast dynamics, is highly sensitive to parameter variations and inverter-induced harmonics, which weakens its performance under disturbed conditions. Fault-tolerant control strategies offer noticeable improvements but often require costly sensors or complex system architectures. As for multiphase machines, they exhibit higher resilience but involve heavy hardware configurations that are difficult to integrate into existing installations. None of these approaches reliably guarantees torque maintenance in the event of severe phase loss [6] [7].

To overcome these limitations, this study introduces an innovative solution: the *Universal Cage Induction Motor* (MACU). This dual-stator machine, featuring both a three-phase winding and a single-phase winding, is capable of automatically reconfiguring its power supply under major grid disturbances. Thanks to this architecture, the MACU exhibits significantly enhanced fault tolerance compared to conventional motors. The natural redistribution of the magnetic field between the two stators ensures the preservation of rotor flux even in the presence of phase loss, thereby maintaining continuous torque and satisfactory mechanical stability [8]-[10].

The paper first develops a comprehensive model of this original structure, incorporating magnetic interactions and the effects of symmetrical components under unbalanced conditions. It then proposes a rotor flux-oriented vector control strategy capable of decoupling flux and torque regulation while integrating an automatic switching mechanism to ensure operation in *ride-through* mode. A detailed theoretical analysis demonstrates the robustness and stability of the proposed method, complemented by experimental validations carried out on a dedicated test bench. These contributions position the MACU as a credible, efficient, and easily integrable solution to ensure service continuity in industrial environments subjected to severe electrical disturbances.

2. State of the Art

2.1. Grid Unbalances: Origin, Modeling, and Impacts

Industrial power systems are often subject to voltage unbalances caused by uneven load distribution, impedance variations, asymmetrical faults, or degraded connections. In weakly interconnected networks, these unbalances can become significant and severely affect sensitive equipment. The analysis of these phenomena relies on symmetrical components, where any unbalanced voltage is decomposed into positive-, negative-, and zero-sequence components. The negative-sequence component is the most critical for induction machines, as it generates a rotating field opposite to the main field, producing an electromagnetic torque oscillating at twice the grid frequency.

This oscillating torque leads to increased currents, winding overheating, and reduced efficiency. The resulting mechanical vibrations can damage the machine, while the instability of the magnetic flux disturbs torque and speed regulation. A severe or prolonged unbalance may thus lead to progressive performance degradation or even an uncontrolled shutdown [11] [12].

2.2. Existing Industrial Solutions and Their Limitations

Several methods have been developed to mitigate the impact of voltage unbalances on induction motors. Scalar control, still widely used due to its simplicity and low cost, quickly becomes unsuitable when voltage conditions no longer satisfy the requirements for maintaining a stable flux, making it unable to compensate for torque oscillations [13].

Direct Torque Control (DTC) provides a more responsive alternative, but its sensitivity to parameter variations and harmonics significantly limits its performance under unbalanced conditions. Even slight distortions degrade control accuracy and amplify torque ripples, particularly when the inverter does not supply high-quality voltage. More advanced approaches, grouped under fault-tolerant control strategies, aim to maintain motor operation despite severe disturbances. These methods often rely on observers, flux estimation, or reconfiguration algorithms. Although effective, they require costly instrumentation, additional sensors, or significant computational resources [14]-[16].

In parallel, the use of multiphase or multi-stator machines provides very high fault tolerance. However, their complexity, cost, and difficult integration into existing installations limit their widespread adoption in industry. These limitations highlight the need for a solution capable of automatically adapting to unbalances while maintaining stable torque and flux, without exceeding economic constraints. It is within this context that the proposed approach is developed, based on the Universal Cage Induction Motor (MACU) and a flux-oriented control strategy designed to enhance resilience against asymmetrical disturbances.

2.3. Fault-Tolerant Architectures

Several architectures have been developed to enhance the robustness of electrical machines against faults. Multiphase motors are among the most widely investigated solutions: increasing the number of phases enables better distribution of electromagnetic stresses and ensures continued operation even in the event of a winding loss. However, these machines require more expensive converters, complex windings, and advanced control electronics, which limit their integration into conventional industrial infrastructures. In addition to hardware-based approaches, various fault-tolerant control strategies have been proposed. Some rely on the dynamic reconfiguration of Direct Torque Control (DTC) to adapt voltage vectors and compensate for unbalances. Although these DTC-FTC methods can maintain torque, they often increase torque ripples and remain sensitive to parameter variations. Other techniques aim to reconstruct a symmetrical voltage through online estimation of symmetrical components, but they require precise instrumentation and significant computational effort. Despite their advancements, these solutions remain limited by their complexity, cost, and difficulty in ensuring long-term stability of flux and torque under severe unbalanced conditions. They also struggle to provide smooth transitions between operating modes or to maintain motor operation in the event of prolonged phase loss [17] [18].

2.4. Vector Control and Limitations under Unbalanced Conditions

Vector control has revolutionized the control of induction machines by enabling a clear decoupling between flux and torque. By transforming stator quantities into a synchronized rotating reference frame, the machine can be controlled as a virtual DC motor, with precise and fast regulation of current components. This technique, widely used in modern drives, offers excellent dynamic performance. However, its effectiveness strongly depends on the estimation of rotor flux, which is difficult to measure directly. Observers based on voltage models perform well at high speeds, whereas those based on current models are more reliable at low speeds. Adaptive approaches combine both models to mitigate the impact of electrical parameter variations. Under unbalanced conditions, vector control must be adapted to account for asymmetrical components. Some studies propose observers capable of extracting positive- and negative-sequence components to correct disturbances in real time. Others rely on signal injection or flux localization techniques to improve

estimation robustness. Although effective, these methods require significant computational power and do not always ensure proper flux maintenance when phase loss becomes severe [6].

2.5. Positioning of the UCIM: Originality and Advantages

The Universal Cage Induction Motor (MACU) adopts a different approach compared to conventional solutions when dealing with unbalanced conditions. Rather than relying solely on complex algorithms or increasing the number of phases, it uses a simple dual-stator architecture combining a three-phase winding with an auxiliary single-phase winding. This configuration provides natural magnetic redundancy, enabling the maintenance of rotor flux and ensuring operational continuity during voltage asymmetries or phase loss. The originality of the MACU lies in its ability to automatically redistribute flux between its two stators, without requiring costly multiphase windings or sophisticated software reconfiguration. Its fault-tolerant capability is inherently based on its electromagnetic structure, making it simpler and more robust than conventional approaches. Coupled with this architecture, rotor flux-oriented control plays a key role by ensuring effective decoupling between flux and torque, allowing stable regulation even under highly unbalanced conditions. The *ride-through* mechanism enables the activation of the auxiliary stator at the appropriate moment to ensure a smooth transition without disturbing the flux. As such, the MACU represents a relevant intermediate solution between multiphase machines, which are often complex and costly, and purely software-based control strategies, which may be insufficient. It combines a streamlined hardware structure, advanced control, and efficient switching to achieve high fault tolerance without excessive technological burden [19] [20].

3. Electromagnetic Description of the MACU

3.1. Physical Description of the MACU

The Universal Cage Induction Motor is characterized by the presence of two stator windings: a main three-phase winding used under normal operating conditions, and an auxiliary single-phase winding designed to ensure service continuity in the event of significant unbalance. These two stators, integrated within the same frame, share a conventional squirrel-cage rotor, giving the machine a hybrid nature that combines three-phase power capability with single-phase backup operation.

Under balanced conditions, the three-phase stator generates the majority of the magnetic flux and allows the motor to deliver its rated torque. When the supply becomes unbalanced or a phase is lost, the single-phase winding, designed to produce sufficient flux, takes over to maintain rotation. This continuity is enabled by the internal magnetic coupling, which ensures coherent interaction between the two winding systems.

3.2. Conceptual Dual-Stator Configuration

The Universal Cage Induction Motor relies on a dual-stator configuration in which

two distinct winding systems coexist within the same magnetic circuit. The three-phase winding occupies the main part of the stator and ensures the generation of the rotating magnetic field during normal operation. The second winding, of single-phase nature, is arranged to produce a flux spatially shifted with respect to the three-phase flux. This shift is achieved by connecting the single-phase winding with a series capacitor, which introduces the necessary electrical phase shift required to generate electromagnetic torque in single-phase mode.

Figure 1 presents a conceptual illustration of this dual-stator architecture. It highlights the arrangement of the windings, the stator geometry, and the main magnetic flux paths. The spatial organization of the two windings allows the motor to naturally transition between conventional three-phase operation and single-phase backup operation, without mechanical modification or structural transformation.

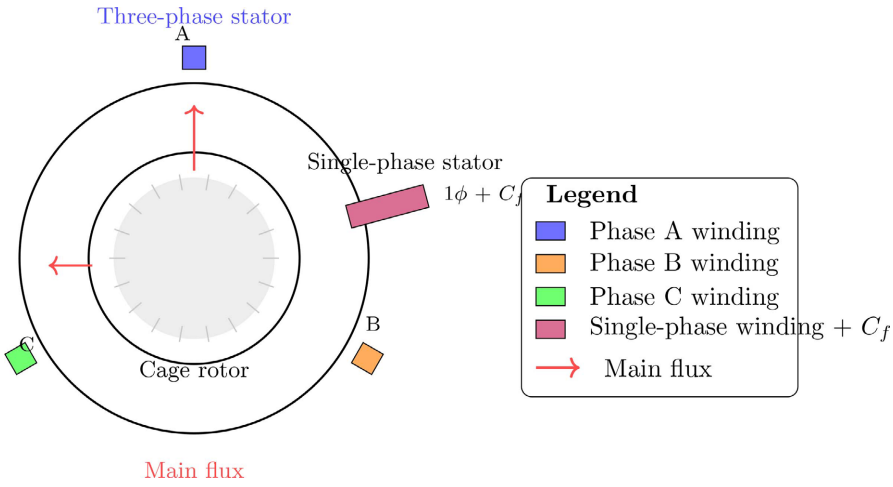

Figure 1. Conceptual diagram of the dual-stator MACU.

This architecture offers remarkable flexibility. When the network is balanced, the rotating field from the three-phase winding dominates the magnetic dynamics. When a phase fails or a severe imbalance occurs, the single-phase winding immediately contributes to maintaining the rotor flux, thus ensuring continuous torque production. The resulting hybrid behavior forms the basis of the MACU's fault-tolerant operation.

3.3. Magnetic Structure and Interactions between Stators

The MACU features two stators sharing the same magnetic core, which results in direct coupling between their fluxes. This coupling is characterized by a mutual inductance that depends on geometry, permeance, and winding orientation. When supplied, the three-phase stator generates a rotating field with angular frequency ω_s that crosses the rotor, induces currents in the cage, and influences the single-phase winding. Conversely, the activation of the single-phase stator produces an alternating flux, less effective in terms of torque production but sufficient to main-

tain rotation and prevent shutdown.

The coexistence of the two systems creates a hybrid magnetic structure in which fluxes overlap and redistribute depending on the power supply conditions. Under normal operation, the three-phase system dominates, whereas under unbalanced conditions, the single-phase winding ensures continuity without any mechanical modification. This magnetic adaptability constitutes the core principle of the MACU fault-tolerant operation.

3.4. Physical Assumptions and Theoretical Framework

The electromagnetic study of the universal cage induction motor is based on a set of assumptions aimed at establishing a consistent mathematical model while preserving the physical validity of the simulated behavior. The machine is assumed to be supplied with sinusoidal signals at the fundamental frequency, which enables the use of the Park transformation and the description of the system in a synchronized rotating reference frame.

The magnetic circuit is assumed to be linear, neglecting saturation and hysteresis effects, with characteristics considered stable at constant temperature. Core losses are neglected, and magnetization and dissipation effects are incorporated into the adopted inductance values. This linearity assumption constitutes a classical approximation in control-oriented models, allowing for a tractable analytical formulation. However, under severe voltage unbalance conditions or during single-phase operation, the spatial distribution of the flux may become non-uniform, leading locally to high flux density levels. In this work, these effects are assumed to remain limited and not to affect the global electromagnetic conversion mechanisms, which are consistent with the flux levels observed in the simulation and experimental validation results presented in Section 7.

The rotor is modeled as a squirrel-cage structure, implying zero rotor voltage in the electrical model, which simplifies the dynamic equations while accurately capturing its transient behavior.

The interactions between the two stators are represented by a mutual inductance, depending on the winding geometry and the magnetic circuit properties. Finally, the electromechanical coupling linking torque to rotor motion is described by classical mechanical equations, taking into account inertia and viscous friction losses.

These assumptions, commonly used in the modeling of induction machines, provide a theoretical framework sufficiently accurate to analyze the behavior of the MACU under unbalanced conditions, while maintaining a level of complexity compatible with the objective of designing a robust control strategy.

4. Complete Mathematical Modeling of the MACU

In this section, the mathematical modeling is first developed for a conventional three-phase induction motor, assuming a single stator-rotor structure. This initial step introduces the fundamental equations in a rotating (dq) reference frame and

establishes the basis for vector control. The extension to the dual-stator MACU case will then be built upon this reference model.

4.1. Transformation $abc \to \alpha\beta \to dq$

The starting point of the modeling is the description of electrical quantities in the natural three-phase reference frame (a,b,c). The stator voltages and currents can be expressed in vector form as follows:

$$\boldsymbol{v}_{sabc} = \begin{bmatrix} v_{sa} \\ v_{sb} \\ v_{sc} \end{bmatrix}, \quad \boldsymbol{i}_{sabc} = \begin{bmatrix} i_{sa} \\ i_{sb} \\ i_{sc} \end{bmatrix}. \tag{1}$$

In a balanced three-phase system with no neutral connection, these quantities satisfy the relation

$$v_{sa} + v_{sb} + v_{sc} = 0, \quad i_{sa} + i_{sb} + i_{sc} = 0. \tag{2}$$

The useful information is thus reduced to two independent components. The Clarke (Concordia) transformation projects the three-phase system onto the (α,β) plane through a linear transformation:

$$\boldsymbol{v}_{s\alpha\beta} = \begin{bmatrix} v_{s\alpha} \\ v_{s\beta} \end{bmatrix} = \boldsymbol{T}_{\alpha\beta}\boldsymbol{v}_{sabc}, \quad \boldsymbol{i}_{s\alpha\beta} = \begin{bmatrix} i_{s\alpha} \\ i_{s\beta} \end{bmatrix} = \boldsymbol{T}_{\alpha\beta}\boldsymbol{i}_{sabc}. \tag{3}$$

The matrix $\boldsymbol{T}_{\alpha\beta}$ is defined to preserve instantaneous power between reference frames. In the three-phase system, this power is expressed as

$$p_s(t) = v_{sa}i_{sa} + v_{sb}i_{sb} + v_{sc}i_{sc}, \tag{4}$$

and in the (α,β) frame as

$$p_s(t) = v_{s\alpha}i_{s\alpha} + v_{s\beta}i_{s\beta}. \tag{5}$$

By enforcing power invariance, one obtains the condition

$$v_{sa}i_{sa} + v_{sb}i_{sb} + v_{sc}i_{sc} = v_{s\alpha}i_{s\alpha} + v_{s\beta}i_{s\beta}, \tag{6}$$

which must hold for any triplet (v_{sa}, v_{sb}, v_{sc}) and (i_{sa}, i_{sb}, i_{sc}) satisfying the neutrality condition. By choosing an orthonormal basis and enforcing zero-sum components, a classical form of the Clarke transformation matrix is given by

$$\boldsymbol{T}_{\alpha\beta} = \sqrt{\frac{2}{3}} \begin{bmatrix} 1 & -\frac{1}{2} & -\frac{1}{2} \\ 0 & \frac{\sqrt{3}}{2} & -\frac{\sqrt{3}}{2} \end{bmatrix}. \tag{7}$$

This transformation performs both dimensionality reduction and energy consistency: the factor $\sqrt{2/3}$ ensures that the vector norm is preserved under equal power conditions.

Once the quantities are expressed in the fixed (α,β) frame, it is useful to introduce a rotating reference frame (d,q) whose orientation is chosen according to a control criterion, such as alignment with the rotor flux. The transformation from the stationary (α,β) frame to the rotating (d,q) frame is achieved

through a rotation of angle $\theta_k(t)$, with angular speed $\omega_k = \mathrm{d}\theta_k/\mathrm{d}t$. One defines

$$\begin{bmatrix} x_d \\ x_q \end{bmatrix} = \boldsymbol{R}(\theta_k)\begin{bmatrix} x_\alpha \\ x_\beta \end{bmatrix}, \tag{8}$$

where $\boldsymbol{R}(\theta_k)$ is the orthogonal rotation matrix given by

$$\boldsymbol{R}(\theta_k) = \begin{bmatrix} \cos\theta_k & \sin\theta_k \\ -\sin\theta_k & \cos\theta_k \end{bmatrix}. \tag{9}$$

By substituting the expression of $\boldsymbol{T}_{\alpha\beta}$, the complete $abc \to dq$ transformation is directly obtained. For a generic quantity x (voltage, current, or flux), one can write

$$\begin{bmatrix} x_d \\ x_q \end{bmatrix} = \boldsymbol{R}(\theta_k)\boldsymbol{T}_{\alpha\beta}\begin{bmatrix} x_a \\ x_b \\ x_c \end{bmatrix}. \tag{10}$$

By combining the two transformations, it is possible to explicitly write

$$\begin{bmatrix} x_d \\ x_q \end{bmatrix} = \sqrt{\frac{2}{3}}\begin{bmatrix} \cos\theta_k & \cos\left(\theta_k - \frac{2\pi}{3}\right) & \cos\left(\theta_k + \frac{2\pi}{3}\right) \\ -\sin\theta_k & -\sin\left(\theta_k - \frac{2\pi}{3}\right) & -\sin\left(\theta_k + \frac{2\pi}{3}\right) \end{bmatrix}\begin{bmatrix} x_a \\ x_b \\ x_c \end{bmatrix}. \tag{11}$$

This corresponds to the standard form of the Park transformation. It is applied identically to stator and rotor voltages, currents, and fluxes, allowing all electrical equations to be expressed in a single rotating reference frame suitable for control design.

4.2. Voltage Equations in the (*dq*) Reference Frame

The voltage equations of a three-phase induction motor can be established in the (a,b,c) reference frame using Kirchhoff's laws applied to each phase. For the stator, one can write

$$v_{sa} = R_s i_{sa} + \frac{\mathrm{d}\psi_{sa}}{\mathrm{d}t},\ v_{sb} = R_s i_{sb} + \frac{\mathrm{d}\psi_{sb}}{\mathrm{d}t},\ v_{sc} = R_s i_{sc} + \frac{\mathrm{d}\psi_{sc}}{\mathrm{d}t}, \tag{12}$$

where R_s denotes the stator resistance per phase, and ψ_{sa}, ψ_{sb}, ψ_{sc} are the flux linkages associated with the stator windings. These relations can be expressed in vector form as

$$\boldsymbol{v}_{sabc} = R_s \boldsymbol{i}_{sabc} + \frac{\mathrm{d}\boldsymbol{\psi}_{sabc}}{\mathrm{d}t}. \tag{13}$$

Applying the Clarke (Concordia) transformation yields the corresponding equations in the (α,β) reference frame:

$$\boldsymbol{v}_{s\alpha\beta} = \boldsymbol{T}_{\alpha\beta}\boldsymbol{v}_{sabc} = R_s \boldsymbol{T}_{\alpha\beta}\boldsymbol{i}_{sabc} + \boldsymbol{T}_{\alpha\beta}\frac{\mathrm{d}\boldsymbol{\psi}_{sabc}}{\mathrm{d}t}. \tag{14}$$

Due to the linearity of the transformation, the order of differentiation and projection can be interchanged, leading to

$$\boldsymbol{v}_{s\alpha\beta} = R_s \boldsymbol{i}_{s\alpha\beta} + \frac{\mathrm{d}\boldsymbol{\psi}_{s\alpha\beta}}{\mathrm{d}t}, \tag{15}$$

with $\boldsymbol{\psi}_{s\alpha\beta} = \boldsymbol{T}_{\alpha\beta}\boldsymbol{\psi}_{sabc}$ and $\boldsymbol{i}_{s\alpha\beta} = \boldsymbol{T}_{\alpha\beta}\boldsymbol{i}_{sabc}$.

The transformation to the rotating (d,q) reference frame requires accounting for the time variation of the reference frame itself. By applying the rotation matrix $\boldsymbol{R}(\theta_k)$, one obtains.

$$\begin{bmatrix} v_{sd} \\ v_{sq} \end{bmatrix} = \boldsymbol{R}(\theta_k)\begin{bmatrix} v_{s\alpha} \\ v_{s\beta} \end{bmatrix}, \begin{bmatrix} \psi_{sd} \\ \psi_{sq} \end{bmatrix} = \boldsymbol{R}(\theta_k)\begin{bmatrix} \psi_{s\alpha} \\ \psi_{s\beta} \end{bmatrix}, \begin{bmatrix} i_{sd} \\ i_{sq} \end{bmatrix} = \boldsymbol{R}(\theta_k)\begin{bmatrix} i_{s\alpha} \\ i_{s\beta} \end{bmatrix}. \tag{16}$$

The time derivative of the stator flux in the (dq) reference frame is not simply the projection of its derivative in the (α,β) frame, since the basis itself is time-varying. One has

$$\frac{\mathrm{d}}{\mathrm{d}t}\begin{bmatrix} \psi_{sd} \\ \psi_{sq} \end{bmatrix} = \frac{\mathrm{d}}{\mathrm{d}t}\left(\boldsymbol{R}(\theta_k)\begin{bmatrix} \psi_{s\alpha} \\ \psi_{s\beta} \end{bmatrix}\right) = \dot{\boldsymbol{R}}(\theta_k)\begin{bmatrix} \psi_{s\alpha} \\ \psi_{s\beta} \end{bmatrix} + \boldsymbol{R}(\theta_k)\frac{\mathrm{d}}{\mathrm{d}t}\begin{bmatrix} \psi_{s\alpha} \\ \psi_{s\beta} \end{bmatrix}. \tag{17}$$

The derivative of the rotation matrix can be expressed as a function of the angular speed $\omega_k = \dot{\theta}_k$. One obtains

$$\dot{\boldsymbol{R}}(\theta_k) = \omega_k\begin{bmatrix} -\sin\theta_k & \cos\theta_k \\ -\cos\theta_k & -\sin\theta_k \end{bmatrix} = \omega_k\begin{bmatrix} 0 & 1 \\ -1 & 0 \end{bmatrix}\boldsymbol{R}(\theta_k), \tag{18}$$

where the matrix

$$\boldsymbol{J} = \begin{bmatrix} 0 & 1 \\ -1 & 0 \end{bmatrix} \tag{19}$$

represents a ninety-degree rotation in the plane. Using this relation, one can write

$$\dot{\boldsymbol{R}}(\theta_k)\begin{bmatrix} \psi_{s\alpha} \\ \psi_{s\beta} \end{bmatrix} = \omega_k\boldsymbol{J}\boldsymbol{R}(\theta_k)\begin{bmatrix} \psi_{s\alpha} \\ \psi_{s\beta} \end{bmatrix} = \omega_k\boldsymbol{J}\begin{bmatrix} \psi_{sd} \\ \psi_{sq} \end{bmatrix}. \tag{20}$$

It follows that

$$\frac{\mathrm{d}}{\mathrm{d}t}\begin{bmatrix} \psi_{sd} \\ \psi_{sq} \end{bmatrix} = \omega_k\boldsymbol{J}\begin{bmatrix} \psi_{sd} \\ \psi_{sq} \end{bmatrix} + \boldsymbol{R}(\theta_k)\frac{\mathrm{d}}{\mathrm{d}t}\begin{bmatrix} \psi_{s\alpha} \\ \psi_{s\beta} \end{bmatrix}. \tag{21}$$

The stator voltage equations in the (α,β) reference frame are written as

$$\begin{bmatrix} v_{s\alpha} \\ v_{s\beta} \end{bmatrix} = R_s\begin{bmatrix} i_{s\alpha} \\ i_{s\beta} \end{bmatrix} + \frac{\mathrm{d}}{\mathrm{d}t}\begin{bmatrix} \psi_{s\alpha} \\ \psi_{s\beta} \end{bmatrix}. \tag{22}$$

Projecting these equations into the (dq) reference frame and using the previous transformations yields

$$\begin{bmatrix} v_{sd} \\ v_{sq} \end{bmatrix} = R_s\begin{bmatrix} i_{sd} \\ i_{sq} \end{bmatrix} + \frac{\mathrm{d}}{\mathrm{d}t}\begin{bmatrix} \psi_{sd} \\ \psi_{sq} \end{bmatrix} - \omega_k\boldsymbol{J}\begin{bmatrix} \psi_{sd} \\ \psi_{sq} \end{bmatrix}. \tag{23}$$

By expanding the contribution of the matrix $\boldsymbol{J}$, this expression can be rewritten in scalar form as

$$v_{sd} = R_s i_{sd} + \frac{\mathrm{d}\psi_{sd}}{\mathrm{d}t} - \omega_k \psi_{sq}, \quad v_{sq} = R_s i_{sq} + \frac{\mathrm{d}\psi_{sq}}{\mathrm{d}t} + \omega_k \psi_{sd}. \tag{24}$$

The same reasoning applies to the rotor equations. In the stator reference frame, the rotor voltages can be written as

$$0 = R_r \boldsymbol{i}_{r\alpha\beta} + \frac{\mathrm{d}\boldsymbol{\psi}_{r\alpha\beta}}{\mathrm{d}t}, \tag{25}$$

since the rotor is short-circuited. In the same rotating (dq) frame with angular speed ω_k, it is necessary to account for the rotor electrical speed ω_r. The slip frequency is then defined as $\omega_{sl} = \omega_k - \omega_r$. By repeating the previous analysis, the rotor voltage equations in the (dq) reference frame become

$$0 = R_r i_{rd} + \frac{\mathrm{d}\psi_{rd}}{\mathrm{d}t} - (\omega_k - \omega_r)\psi_{rq}, \quad 0 = R_r i_{rq} + \frac{\mathrm{d}\psi_{rq}}{\mathrm{d}t} + (\omega_k - \omega_r)\psi_{rd}. \tag{26}$$

These relations complete the formulation of the voltage equations in the rotating reference frame. They constitute the foundation from which the flux equations, torque expression, and the dual-stator MACU model under unbalanced conditions will be derived in the following subsections.

4.3. Flux Equations

Electromagnetic fluxes constitute the fundamental link between voltages, currents, and energy. In an induction motor, stator and rotor fluxes are described by inductive relationships connecting currents to self and mutual inductances. These equations are initially formulated in the three-phase (a,b,c) reference frame and then expressed in the (dq) frame. For the stator:

$$\psi_{sd} = L_s i_{sd} + L_m i_{rd}, \quad \psi_{sq} = L_s i_{sq} + L_m i_{rq}, \tag{27}$$

where L_s is the stator self-inductance and L_m is the mutual inductance. For the rotor:

$$\psi_{rd} = L_m i_{sd} + L_r i_{rd}, \quad \psi_{rq} = L_m i_{sq} + L_r i_{rq}, \tag{28}$$

with L_r denoting the rotor self-inductance.

These relations, derived from the linear magnetic model, describe the bidirectional coupling between stator and rotor. They show that the d - and q -axis flux components directly depend on the currents, with the mutual inductance L_m playing a key role in flux transfer and in the overall dynamic behavior of the motor.

4.4. Analytical Elimination of Rotor Currents

The objective of this step is to express the entire motor dynamics solely in terms of stator quantities and rotor fluxes, in order to facilitate analysis and control design. The rotor currents i_{rd} and i_{rq} are eliminated using the previously established flux equations. By rewriting these equations in matrix form, one obtains.

$$\begin{bmatrix} \psi_{rd} \\ \psi_{rq} \end{bmatrix} = L_m \begin{bmatrix} i_{sd} \\ i_{sq} \end{bmatrix} + L_r \begin{bmatrix} i_{rd} \\ i_{rq} \end{bmatrix}, \tag{29}$$

which allows the rotor currents to be isolated as

$$\begin{bmatrix} i_{rd} \\ i_{rq} \end{bmatrix} = \frac{1}{L_r}\left(\begin{bmatrix} \psi_{rd} \\ \psi_{rq} \end{bmatrix} - L_m \begin{bmatrix} i_{sd} \\ i_{sq} \end{bmatrix}\right). \tag{30}$$

This relation introduces a direct dependence of the rotor currents on the associated fluxes. By differentiating this expression and substituting it into the rotor voltage equations established in the (dq) reference frame, an explicit dynamic model of the rotor fluxes can be obtained. Substituting into the rotor equations

$$0 = R_r i_{rd} + \frac{\mathrm{d}\psi_{rd}}{\mathrm{d}t} - (\omega_k - \omega_r)\psi_{rq}, \quad 0 = R_r i_{rq} + \frac{\mathrm{d}\psi_{rq}}{\mathrm{d}t} + (\omega_k - \omega_r)\psi_{rd}, \tag{31}$$

leads, after simplification, to

$$\frac{\mathrm{d}\psi_{rd}}{\mathrm{d}t} = -\frac{R_r}{L_r}\psi_{rd} + \omega_{sl}\psi_{rq} + \frac{L_m R_r}{L_r} i_{sd}, \tag{32}$$

$$\frac{\mathrm{d}\psi_{rq}}{\mathrm{d}t} = -\frac{R_r}{L_r}\psi_{rq} - \omega_{sl}\psi_{rd} + \frac{L_m R_r}{L_r} i_{sq}, \tag{33}$$

where the slip angular frequency is defined as $\omega_{sl} = \omega_k - \omega_r$. These equations describe the time evolution of the rotor fluxes under the influence of stator currents and slip. They constitute a fundamental result for the development of rotor flux-oriented control.

4.5. Final Dynamic Equations and State-Space Representation

The stator voltage equations in the (dq) reference frame, combined with the flux model, allow the complete dynamic system of the motor to be established. By grouping the different expressions, the stator relations are first written as

$$v_{sd} = R_s i_{sd} + \frac{\mathrm{d}\psi_{sd}}{\mathrm{d}t} - \omega_k \psi_{sq}, \quad v_{sq} = R_s i_{sq} + \frac{\mathrm{d}\psi_{sq}}{\mathrm{d}t} + \omega_k \psi_{sd}. \tag{34}$$

By substituting the stator fluxes expressed in terms of currents and rotor fluxes, and by introducing the previously derived rotor flux dynamics, the entire model can be written in a compact matrix form. By choosing the state variables as

$$\boldsymbol{x} = \begin{bmatrix} i_{sd} \\ i_{sq} \\ \psi_{rd} \\ \psi_{rq} \end{bmatrix}, \tag{35}$$

the dynamic system can be expressed in the general form

$$\frac{\mathrm{d}\boldsymbol{x}}{\mathrm{d}t} = \boldsymbol{A}(\omega_k, \omega_r)\boldsymbol{x} + \boldsymbol{B}\boldsymbol{v}_s, \tag{36}$$

where $\boldsymbol{v}_s = \begin{bmatrix} v_{sd} \\ v_{sq} \end{bmatrix}$ represents the stator voltage vector. The dynamic matrix $\boldsymbol{A}$ includes terms associated with resistances, inductances, cross-couplings, and gyroscopic effects induced by the rotating reference frame. Its general structure is given by

$$\boldsymbol{A}=\begin{bmatrix} -\frac{R_s}{L_s}-\frac{L_m^2 R_r}{L_s L_r^2} & \omega_k & \frac{L_m R_r}{L_s L_r} & 0 \\ -\omega_k & -\frac{R_s}{L_s}-\frac{L_m^2 R_r}{L_s L_r^2} & 0 & \frac{L_m R_r}{L_s L_r} \\ \frac{L_m R_r}{L_r} & 0 & -\frac{R_r}{L_r} & \omega_{sl} \\ 0 & \frac{L_m R_r}{L_r} & -\omega_{sl} & -\frac{R_r}{L_r} \end{bmatrix}. \tag{37}$$

The matrix $\boldsymbol{B}$, which relates the stator voltages to the state derivatives, is given by

$$\boldsymbol{B}=\frac{1}{L_s}\begin{bmatrix} 1 & 0 \\ 0 & 1 \\ 0 & 0 \\ 0 & 0 \end{bmatrix}. \tag{38}$$

This set of equations constitutes the complete state-space representation of the induction machine in the (dq) reference frame. It provides an analytical framework for designing advanced vector control strategies, such as the rotor flux-oriented control used in this work. It will also serve as the basis for extending the model to the dual-stator MACU, developed in the following section.

4.6. Coupled Dual-Stator Model

The Universal Cage Induction Motor is characterized by the presence of two stator windings: a main three-phase winding $s_{3\phi}$ and an auxiliary single-phase winding $s_{1\phi}$. These two stators share the same magnetic circuit and interact directly with the rotor. The model must therefore incorporate both the self-inductances of each winding and the mutual inductances that couple them, leading to a matrix formulation of the fluxes.

Let $\boldsymbol{i}_{s,3\phi}$ denote the vector of three-phase stator currents, $i_{s,1\phi}$ the single-phase current, and $\boldsymbol{i}_r$ the rotor currents expressed in the (dq) reference frame. The fluxes can then be written in compact form as

$$\begin{bmatrix} \boldsymbol{\psi}_{s,3\phi} \\ \psi_{s,1\phi} \\ \boldsymbol{\psi}_r \end{bmatrix}=\begin{bmatrix} L_{s,3\phi} & M_{sm} & L_{m,3\phi} \\ M_{sm} & L_{s,1\phi} & L_{m,1\phi} \\ L_{m,3\phi}^{\top} & L_{m,1\phi}^{\top} & L_r \end{bmatrix}\begin{bmatrix} \boldsymbol{i}_{s,3\phi} \\ i_{s,1\phi} \\ \boldsymbol{i}_r \end{bmatrix}. \tag{39}$$

This global inductance matrix of the MACU includes:

- $L_{s,3\phi}$: self and mutual inductances of the three-phase stator,
- $L_{s,1\phi}$: self-inductance of the single-phase stator,
- M_{sm}: direct coupling between the two stators,
- $L_{m,3\phi}$ and $L_{m,1\phi}$: mutual inductances linking each stator to the rotor.

This representation highlights the hybrid nature of the MACU: the three-phase and single-phase fluxes are interdependent through the magnetic circuit permeance. It allows for an accurate evaluation of the contribution of each winding depending

on the supply mode.

4.7. Demonstration of Magnetic Coupling

The coupling between the stator windings of the MACU arises from the fact that they share the same ferromagnetic core. When one winding is energized, part of the generated magnetic flux propagates through the regions occupied by the other winding, in accordance with electromagnetic laws governing magnetic circuits. For the three-phase winding, the generated flux can be expressed as:

$$\phi_{3\phi} = \Lambda_{3\phi} i_{s,3\phi} \tag{40}$$

and a portion of this flux is intercepted by the single-phase winding:

$$\phi_{1\phi} = k_m \phi_{3\phi}, \quad \psi_{s,1\phi} = M_{sm} i_{s,3\phi}. \tag{41}$$

Conversely, when the single-phase winding is supplied, it produces:

$$\phi_{1\phi} = \Lambda_{1\phi} i_{s,1\phi}, \quad \psi_{s,3\phi} = M_{sm} i_{s,1\phi}, \tag{42}$$

which confirms the bidirectional nature of the mutual inductance M_{sm}.

The value of M_{sm} depends on geometric parameters (winding positions, slot and tooth dimensions, magnetic path length), as well as on the presence of the capacitor in the single-phase winding, which affects the flux distribution. Strictly speaking, this mutual inductance may also depend on the operating point, particularly under severe unbalanced conditions where the spatial distribution of the magnetic field becomes non-uniform, leading to cross-saturation effects and spatial harmonics.

In this work, M_{sm} is assumed to be constant, which constitutes a common approximation in analytical modeling. This assumption allows for a compact formulation while capturing the dominant mechanisms of magnetic coupling. The possible variations of M_{sm} are considered to be of secondary order and do not significantly affect the overall system dynamics, as supported by the simulation and experimental validation results presented in Section 7.

In certain configurations, the coupling becomes significant and must be explicitly included in the inductance matrix.

This analysis highlights that the MACU cannot be modeled as two independent systems: the flux produced by each winding directly influences the dynamics of the other, giving this hybrid machine a distinctive electromagnetic structure that is fundamental to its fault-tolerant operation.

4.8. Capacitor Effect and Phase-Shift Modeling

The single-phase operating mode of the MACU uses a series capacitor in the auxiliary winding. This component creates a current phase shift with respect to the applied voltage, generating a non-collinear flux that is essential for torque production and for maintaining rotor rotation. Let the voltage applied to the single-phase winding be expressed as.

$$v_{s,1\phi}(t) = V_m \cos(\omega_s t), \tag{43}$$

where V_m denotes the amplitude and ω_s the fundamental angular frequency of the supply. The current flowing through the capacitor is given by

$$i_C(t) = C_f \frac{\mathrm{d}v_{s,1\phi}}{\mathrm{d}t} = -C_f \omega_s V_m \sin(\omega_s t), \tag{44}$$

so that the total current in the single-phase winding can be modeled as

$$i_{s,1\phi}(t) = I_m \cos(\omega_s t + \varphi_C), \tag{45}$$

where φ_C represents the phase shift induced by the capacitor. A simple analysis of the series single-phase circuit $(R_{s,1\phi}, L_{s,1\phi}, C_f)$ yields

$$\tan(\varphi_C) = \frac{\omega_s L_{s,1\phi} - \dfrac{1}{\omega_s C_f}}{R_{s,1\phi}}. \tag{46}$$

When the capacitor is sized such that

$$\omega_s L_{s,1\phi} - \frac{1}{\omega_s C_f} \approx R_{s,1\phi}, \tag{47}$$

the phase shift approaches $\varphi_C \approx \pi/2$, thereby maximizing the torque-producing effect. The flux generated by the single-phase winding can then be written as

$$\psi_{1\phi}(t) = L_{s,1\phi} i_{s,1\phi}(t), \tag{48}$$

and its spatial projection differs from that of the three-phase flux due to the introduced temporal phase shift. Consequently, even when the three-phase rotating field deteriorates or disappears, the single-phase winding remains capable of producing a complementary flux sufficient to maintain a torque component. This phase-shift modeling constitutes a key element of the MACU robustness, as it ensures a minimum level of operation even in the event of phase loss, without requiring an external inverter or complex control devices.

4.9. Automatic Three-Phase/Single-Phase Reconfiguration

The MACU is characterized by its ability to naturally transition from normal three-phase operation to a single-phase backup mode. This transition is not merely a change in power supply but results from the electromagnetic coupling between the stators. In the presence of unbalance or phase loss, the positive-sequence component of the field weakens while the negative-sequence component becomes dominant, reducing the average torque. The addition of the single-phase flux, phase-shifted by the capacitor, makes it possible to preserve a useful component of the rotor flux:

$$\boldsymbol{\psi}_{s,3\phi} = \boldsymbol{\psi}_s^{(+)} + \boldsymbol{\psi}_s^{(-)} \tag{49}$$

$$\boldsymbol{\psi}_r = L_m \left(\boldsymbol{i}_{s,3\phi} + k_m i_{s,1\phi} \right) \tag{50}$$

When the unbalance becomes severe, $i_{s,1\phi}$ becomes predominant and stabilizes the flux. The rotor dynamics can then be expressed as:

$$\frac{\mathrm{d}\psi_r}{\mathrm{d}t} = -\frac{R_r}{L_r}\psi_r + \frac{L_m R_r}{L_r}\left(i_{sd} + k_m i_{s,1\phi} \right) \tag{51}$$

The single-phase current thus compensates for the loss of i_{sd}, ensuring continuity of flux and torque without mechanical switching or dedicated control. This property can be effectively exploited by the IRFO strategy to maintain stability under disturbed conditions.

4.10. Symmetrical Components Decomposition

The analysis of voltage unbalance relies on the theory of symmetrical components. Any three-phase system, even if unbalanced, can be expressed as the sum of positive-, negative-, and possibly zero-sequence components.

For phase voltages V_a, V_b, V_c and the operator $a = \mathrm{e}^{j\frac{2\pi}{3}}$ satisfying $1 + a + a^2 = 0$, the components are defined as:

$$V^{(+)} = \frac{1}{3}\left(V_a + aV_b + a^2V_c\right), \tag{52}$$

$$V^{(-)} = \frac{1}{3}\left(V_a + a^2V_b + aV_c\right), \tag{53}$$

$$V^{(0)} = \frac{1}{3}\left(V_a + V_b + V_c\right). \tag{54}$$

The reconstruction of the phase voltages is given by:

$$\begin{bmatrix} V_a \\ V_b \\ V_c \end{bmatrix} = \begin{bmatrix} 1 & 1 & 1 \\ 1 & a^2 & a \\ 1 & a & a^2 \end{bmatrix} \begin{bmatrix} V^{(0)} \\ V^{(+)} \\ V^{(-)} \end{bmatrix}. \tag{55}$$

In the absence of a neutral connection, the zero-sequence component vanishes, and only the positive- and negative-sequence components remain, corresponding to two rotating fields of opposite directions at angular frequency ω_s. The level of unbalance is quantified by:

$$k_U = \frac{\left|V^{(-)}\right|}{\left|V^{(+)}\right|}. \tag{56}$$

A low value of k_U indicates a minor disturbance, whereas a high value reflects a severe unbalance that may compromise motor stability.

4.11. Analytical Expression of the Pulsating Torque at $2\omega_s$

The electromagnetic torque of an induction motor in the (dq) reference frame is given by:

$$T_e = \frac{3}{2}p\left(\psi_{sd}i_{sq} - \psi_{sq}i_{sd}\right). \tag{57}$$

Under balanced conditions with rotor flux orientation, one imposes $\psi_{sq} = 0$, which leads to $T_e \propto \psi_r i_{sq}$. In the presence of unbalance, the stator quantities can be decomposed into positive- and negative-sequence components, generating two rotating fields in opposite directions. The stator current can then be expressed as:

$$\underline{I}_s(t) = \underline{I}^{(+)} e^{j\omega_s t} + \underline{I}^{(-)} e^{-j\omega_s t}. \tag{58}$$

The resulting torque takes the form:

$$T_e(t) = \overline{T}_e + \Delta T_e \cos(2\omega_s t + \varphi), \tag{59}$$

where $\overline{T}_e$ is the average torque and ΔT_e is the amplitude of the pulsation, related to the product of the positive- and negative-sequence components. For moderate unbalance:

$$\Delta T_e \approx 2k_U \overline{T}_e. \tag{60}$$

This relationship shows that the unbalance factor k_U directly determines the magnitude of torque oscillations, which induce mechanical vibrations at $2\omega_s$, leading to noise, fatigue, and reduced lifetime. Their mitigation is therefore a key objective in MACU control design.

4.12. Energy Analysis under Unbalanced Conditions

Unbalance does not only induce torque oscillations; it also alters power distribution and reduces overall efficiency. The instantaneous stator power is given by:

$$p_s(t) = v_{sa} i_{sa} + v_{sb} i_{sb} + v_{sc} i_{sc}, \tag{61}$$

or, in the (α, β) frame:

$$p_s(t) = v_{s\alpha} i_{s\alpha} + v_{s\beta} i_{s\beta}. \tag{62}$$

The positive-sequence component contributes to useful torque, whereas the negative-sequence component generates additional currents that increase Joule losses. The stator and rotor copper losses are expressed as:

$$p_{cu,s}(t) = 3R_s \left(i_{sd}^2 + i_{sq}^2\right), \tag{63}$$

$$p_{cu,r}(t) = 3R_r \left(i_{rd}^2 + i_{rq}^2\right). \tag{64}$$

The mechanical power is given by:

$$p_m(t) = T_e(t)\,\omega_m(t), \tag{65}$$

and the instantaneous efficiency is:

$$\eta(t) = \frac{p_m(t)}{p_s(t)}. \tag{66}$$

Thus, unbalance increases losses, induces fluctuations in mechanical power, and degrades efficiency. The dual-stator architecture and control strategy of the MACU aim to mitigate the impact of the negative-sequence component in order to preserve energy performance.

5. MACU IRFO Ride-Through Control

The IRFO (*Indirect Rotor Field Orientation*) control strategy consists of defining a rotating reference frame in which the rotor flux is aligned with the direct axis, imposing $\psi_{rq} = 0$. In this framework, i_{sd} controls the flux while i_{sq} determines the torque, thus transforming the induction machine into a system equivalent to a DC machine, where flux and torque are independently controlled. This orienta-

tion enables effective control even under unbalanced supply conditions, thanks to the estimation of the angle θ_k, which continuously adapts the (dq) reference frame to the actual position of the rotor flux.

5.1. Demonstration of Flux/Torque Decoupling

The decoupling is established by considering the dynamic equations with $\psi_{rq} = 0$. The direct-axis flux dynamics are given by:

$$\frac{\mathrm{d}\psi_r}{\mathrm{d}t} = -\frac{R_r}{L_r}\psi_r + \frac{L_m R_r}{L_r} i_{sd}, \tag{67}$$

showing that only i_{sd} influences the flux. The quadrature component is expressed as:

$$\frac{\mathrm{d}\psi_{rq}}{\mathrm{d}t} = -\frac{R_r}{L_r}\psi_{rq} - \omega_{sl}\psi_r + \frac{L_m R_r}{L_r} i_{sq}. \tag{68}$$

By imposing $\psi_{rq} = 0$, one obtains:

$$\omega_{sl}\psi_r = \frac{L_m R_r}{L_r} i_{sq}. \tag{69}$$

This relation demonstrates that i_{sq} exclusively governs the torque without affecting the flux. The IRFO control thus ensures a clear decoupling between i_{sd} and i_{sq}, guaranteeing stability even under unbalanced conditions.

5.2. Slip Expression

The slip angular frequency is given by

$$\omega_{sl} = \frac{L_m R_r}{L_r \psi_r} i_{sq}. \tag{70}$$

This classical IRFO relationship shows that ω_{sl} is proportional to the quadrature current i_{sq}, which is responsible for torque production. The flux orientation imposes:

$$\omega_k = \omega_r + \omega_{sl}. \tag{71}$$

The slip tends to zero near synchronous mechanical speed but increases under load or during transient conditions. Its definition based on rotor flux remains valid even under unbalanced conditions, thereby enhancing control robustness.

5.3. Electromagnetic Torque Expression

The general torque expression in the (dq) reference frame is given by:

$$T_e = \frac{3}{2} p \left(\psi_{sd} i_{sq} - \psi_{sq} i_{sd} \right). \tag{72}$$

With the stator flux expressions:

$$\psi_{sd} = L_s i_{sd} + L_m i_{rd}, \quad \psi_{sq} = L_s i_{sq} + L_m i_{rq}, \tag{73}$$

and by imposing $\psi_{rq} = 0$, $\psi_{rd} = \psi_r$, the torque expression simplifies to:

$$T_e = \frac{3}{2} p \frac{L_m}{L_r} \psi_r i_{sq}. \tag{74}$$

The torque is therefore directly proportional to the rotor flux ψ_r and the quadrature current i_{sq}, while i_{sd} regulates only the flux. This decoupling makes the control simpler and more effective, even in the presence of voltage asymmetries, and constitutes a key advantage for the MACU Ride-Through strategy.

5.4. Flux Control Loop

Rotor flux regulation is at the core of IRFO control. The dynamic equation:

$$\frac{\mathrm{d}\psi_r}{\mathrm{d}t} = -\frac{R_r}{L_r}\psi_r + \frac{L_m R_r}{L_r} i_{sd} \tag{75}$$

shows that the flux depends only on i_{sd} in the aligned reference frame, with a time constant $\tau_r = L_r / R_r$. To impose a reference value $\psi_r^\star$, the direct current reference is given by:

$$i_{sd}^\star = \frac{\psi_r^\star}{L_m}. \tag{76}$$

A PI controller adjusts $i_{sd}^\star$ in real time to ensure flux convergence despite parameter variations or grid unbalances.

5.5. Torque Control Loop

The oriented electromagnetic torque is expressed as:

$$T_e = \frac{3}{2} p \frac{L_m}{L_r} \psi_r i_{sq}. \tag{77}$$

Thus, for a given flux, the torque depends linearly on i_{sq}. The quadrature current reference is obtained by inversion:

$$i_{sq}^\star = \frac{2}{3} \frac{L_r}{p L_m} \frac{T_e^\star}{\psi_r}. \tag{78}$$

A current controller corrects the error $i_{sq}^\star - i_{sq}$, ensuring a fast and stable response even in the presence of disturbances. Thanks to flux/torque decoupling, the control maintains strong robustness under unbalanced conditions.

5.6. Dynamic Compensation

The voltage equations in the (dq) reference frame include cross-coupling terms related to rotation, responsible for the interaction between direct and quadrature axes:

$$v_{sd} = R_s i_{sd} + \frac{\mathrm{d}\psi_{sd}}{\mathrm{d}t} - \omega_k \psi_{sq}, \quad v_{sq} = R_s i_{sq} + \frac{\mathrm{d}\psi_{sq}}{\mathrm{d}t} + \omega_k \psi_{sd}. \tag{79}$$

These interactions are compensated by redefining the control voltages, after expanding the stator flux expressions and imposing $\psi_{rq} = 0$:

$$v'_{sd} = v_{sd} + \omega_k L_s i_{sq}, \quad v'_{sq} = v_{sq} - \omega_k L_s i_{sd} - \omega_k \psi_r. \tag{80}$$

Thus, the model reduces to two independent first-order systems, enabling classical current controller design and ensuring stable response even under distorted

voltage conditions.

5.7. Flux Observer

The IRFO control requires a reliable estimation of the rotor flux ψ_r. This flux is evaluated from the dynamic equation:

$$\frac{\mathrm{d}\psi_r}{\mathrm{d}t} = -\frac{R_r}{L_r}\psi_r + \frac{L_m R_r}{L_r} i_{sd}, \tag{81}$$

and from the reconstructed stator flux:

$$\boldsymbol{\psi}_s(t) = \int_0^t \left(\boldsymbol{v}_s - R_s \boldsymbol{i}_s\right) \mathrm{d}t. \tag{82}$$

The observer corrects the estimation as follows:

$$\frac{\mathrm{d}\hat{\psi}_r}{\mathrm{d}t} = -\frac{R_r}{L_r}\hat{\psi}_r + \frac{L_m R_r}{L_r} i_{sd} + K_o\left(\psi_s - \hat{\psi}_s\right), \tag{83}$$

where K_o is the observer gain. The estimation error $e_\psi = \psi_r - \hat{\psi}_r$ evolves as:

$$\frac{\mathrm{d}e_\psi}{\mathrm{d}t} = -\left(\frac{R_r}{L_r} + K_o\right) e_\psi, \tag{84}$$

ensuring exponential convergence as long as $K_o > 0$. An appropriate choice of K_o guarantees both stability and fast convergence, whereas an excessively high value makes the estimation sensitive to noise. This observer is essential for maintaining IRFO control accuracy and ensuring MACU robustness in Ride-Through operation.

5.8. Unbalance Detection

The Ride-Through strategy relies on rapid detection of voltage unbalance in order to adapt the control and switch to single-phase mode when necessary. The decomposition into symmetrical components allows this phenomenon to be quantified by the ratio:

$$k_U = \frac{\left|V^{(-)}\right|}{\left|V^{(+)}\right|}. \tag{85}$$

A low value of k_U indicates a nearly balanced supply, whereas a high value reflects a significant negative-sequence component generating torque oscillations. The analysis of stator voltages, transformed into the (α, β) frame, enables real-time estimation of these components and triggers reconfiguration when k_U exceeds a critical threshold $k_{U,\mathrm{crit}}$.

5.9. Three-Phase → Single-Phase Switching Algorithm

When the voltage unbalance factor k_U exceeds a critical threshold $k_{U,\mathrm{crit}}$, the three-phase rotating field becomes severely distorted, compromising torque production. To ensure continuity of operation, a progressive switching mechanism toward the single-phase winding is implemented. The transition is governed by a weighting

coefficient $\alpha(k_U) \in [0,1]$ defined as:

$$\alpha(k_U) = \begin{cases} 0 & \text{if } k_U \le k_{U,\text{crit}} \\ \dfrac{k_U - k_{U,\text{crit}}}{k_{U,\max} - k_{U,\text{crit}}} & \text{if } k_{U,\text{crit}} < k_U < k_{U,\max} \\ 1 & \text{if } k_U \ge k_{U,\max} \end{cases} \tag{86}$$

The current references are then defined by interpolation:

$$\boldsymbol{i}_{s,3\phi}^{ref} = (1-\alpha)\boldsymbol{i}_{s,3\phi}^{nom}, \quad i_{s,1\phi}^{ref} = \alpha i_{s,1\phi}^{nom} \tag{87}$$

where $\boldsymbol{i}_{s,3\phi}^{nom}$ and $i_{s,1\phi}^{nom}$ denote the nominal current references under three-phase and single-phase operation, respectively. These nominal references are generated by the IRFO control scheme, ensuring consistent flux regulation during the transition. To prevent oscillatory switching around the threshold, a hysteresis band Δk_U is introduced:

$$\begin{cases} \text{activation of degraded mode if } k_U > k_{U,\text{crit}} + \Delta k_U \\ \text{return to three-phase mode if } k_U < k_{U,\text{crit}} - \Delta k_U \end{cases} \tag{88}$$

Furthermore, the variation of α is constrained by a rate limiter:

$$\left| \frac{\mathrm{d}\alpha}{\mathrm{d}t} \right| \le r_{\max} \tag{89}$$

to ensure a smooth transition and avoid abrupt transients in flux and torque. Thanks to the mutual inductance between the stator windings, this mechanism ensures a continuous transfer of magnetic flux without discontinuity, allowing a sufficient residual torque to be maintained and preventing the driven load from stalling.

5.10. Flux and Torque Continuity during Transition

Maintaining rotor flux continuity is essential for the Ride-Through strategy. During unbalanced conditions, the positive-sequence component of the three-phase voltage decreases, but the magnetic inertia of the flux, associated with its relatively large time constant, allows operation to be sustained during the transition to single-phase mode. The flux dynamics can be written as:

$$\frac{\mathrm{d}\psi_r}{\mathrm{d}t} = -\frac{R_r}{L_r}\psi_r + \frac{L_m R_r}{L_r}\left(i_{sd} + k_m i_{s,1\phi}\right). \tag{90}$$

The term $k_m i_{s,1\phi}$ compensates for the reduction of i_{sd} and prevents a sudden drop in flux, thereby ensuring torque continuity. The IRFO control adjusts the current references to preserve the alignment of the (dq) frame and maintain a usable torque through i_{sq}, even under prolonged disturbances.

5.11. Stability Analysis of the Complete System

Stability in Ride-Through mode is studied by linearizing the system around an operating point:

$$\Delta\dot{\boldsymbol{x}} = \boldsymbol{A}_{\text{eq}}\Delta\boldsymbol{x}. \tag{91}$$

The matrix A_{eq} includes speed, mutual inductances, and rotor resistance. Stability requires that all its eigenvalues have negative real parts. The quadrature-axis dynamics can be expressed as:

$$\Delta \dot{i}_{sq} = -\left(\frac{R_s}{L_s} + \frac{pL_m\bar{\psi}_r}{JL_r}\right)\Delta i_{sq} - \frac{B}{J}\Delta\omega_m. \tag{92}$$

The stability condition then becomes:

$$\frac{pL_m\bar{\psi}_r}{JL_r} < \frac{R_s}{L_s} + \frac{B}{J}. \tag{93}$$

This inequality imposes that the torque loop remains moderate relative to dissipative effects. The single-phase stator slightly modifies these coefficients without compromising stability, provided that the controller gains are properly tuned.

Thus, the MACU with IRFO control maintains stable and robust behavior, ensuring torque production even under severe unbalanced conditions.

6. Advanced Theoretical Analysis

6.1. Energy Analysis: Losses, Efficiency, and Stability

The energy behavior of the motor under disturbed conditions is a key factor in assessing its stability. The instantaneous stator power is expressed as:

$$p_s(t) = v_{sa}i_{sa} + v_{sb}i_{sb} + v_{sc}i_{sc}, \tag{94}$$

or, in the (α,β) frame:

$$p_s(t) = v_{s\alpha}i_{s\alpha} + v_{s\beta}i_{s\beta}. \tag{95}$$

Under unbalanced conditions, the positive-sequence component contributes to useful torque, whereas the negative-sequence component generates additional currents, leading to increased Joule losses. The copper losses are given by:

$$p_{cu,s}(t) = 3R_s\left(i_{sd}^2 + i_{sq}^2\right),\ \ p_{cu,r}(t) = 3R_r\left(i_{rd}^2 + i_{rq}^2\right). \tag{96}$$

The mechanical power is expressed as:

$$p_m(t) = T_e(t)\omega_m(t), \tag{97}$$

and the instantaneous efficiency as:

$$\eta(t) = \frac{p_m(t)}{p_s(t)}. \tag{98}$$

Torque oscillations at $2\omega_s$ induce power fluctuations and reduce efficiency, which justifies the use of compensation strategies and Ride-Through operation.

6.2. Frequency Analysis: Harmonics and Negative Sequence

Spectral analysis of stator currents reveals the presence of harmonics. Under balanced conditions, the currents are dominated by the fundamental component at ω_s and a few harmonics introduced by PWM. In the presence of unbalance, a component at $-\omega_s$ appears:

$$i_s(t) = I^{(+)}e^{j\omega_s t} + I^{(-)}e^{-j\omega_s t} + \sum_{k\geq 3} I_k e^{jk\omega_s t}. \quad (99)$$

This negative-sequence component, proportional to the unbalance factor k_U, generates torque oscillations at $2\omega_s$, increases harmonic distortion, and degrades torque smoothness. Harmonics of orders 5 and 7, typically introduced by the inverter, remain secondary compared to the impact of voltage unbalance. The IRFO control, through flux orientation and dynamic compensation, mitigates the effect of these parasitic components and preserves waveform quality close to that of balanced operation.

6.3. Pulsating Torque Analysis

The electromagnetic torque in the (dq) reference frame is expressed as:

$$T_e(t) = \frac{3}{2} p\left(\psi_{sd} i_{sq} - \psi_{sq} i_{sd}\right). \quad (100)$$

Under unbalanced conditions, the stator current can be decomposed into positive- and negative-sequence components:

$$\underline{I}_s(t) = I^{(+)}e^{j\omega_s t} + I^{(-)}e^{-j\omega_s t}. \quad (101)$$

The resulting torque consists of an average component and an oscillating term:

$$T_e(t) = \overline{T}_e + \Delta T_e \cos\left(2\omega_s t + \varphi\right), \quad (102)$$

with

$$\Delta T_e \approx 2k_U \overline{T}_e. \quad (103)$$

Thus, even a small unbalance produces oscillations at $2\omega_s$, leading to vibrations, noise, and mechanical wear. The IRFO control of the MACU mitigates these effects by stabilizing the rotor flux and limiting the contribution of the negative-sequence component.

6.4. Small-Signal Stability Analysis

Local stability is analyzed by linearizing the system around an operating point defined by $\overline{i}_{sd}$, $\overline{i}_{sq}$, $\overline{\psi}_r$, $\overline{\omega}_m$. The perturbations are:

$$\Delta i_{sd},\ \Delta i_{sq},\ \Delta\psi_r,\ \Delta\omega_m, \quad (104)$$

and the dynamics can be written as:

$$\Delta\dot{\boldsymbol{x}} = \boldsymbol{A}_{\text{eq}}\Delta\boldsymbol{x}. \quad (105)$$

The matrix $\boldsymbol{A}_{\text{eq}}$ includes resistances, inductances, slip, and direct/quadrature coupling terms. Stability is ensured if all eigenvalues have negative real parts.

Copper losses and viscous friction enhance dissipation, while the electromagnetic torque may either stabilize or destabilize the system depending on the operating point. The flux/torque decoupling imposed by IRFO ensures stable internal dynamics and convergence of the state variables toward their nominal values.

6.5. Analytical Conditions for Stable Switching

The transition from three-phase to single-phase operation must preserve system

stability, as it directly depends on the dynamics of the rotor flux. When the voltage unbalance becomes critical, the contribution of the three-phase winding decreases while that of the single-phase winding increases. To avoid abrupt variations in ψ_r, it is necessary to ensure the continuity of the equivalent current:

$$\frac{\mathrm{d}\psi_r}{\mathrm{d}t} = -\frac{R_r}{L_r}\psi_r + \frac{L_m R_r}{L_r}\left(i_{sd} + k_m i_{s,1\phi}\right), \tag{106}$$

$$i_{sd}^{(\mathrm{eq})}(t) = i_{sd}(t) + k_m i_{s,1\phi}(t). \tag{107}$$

The stability condition is expressed as:

$$\lim_{t\to t_0^-} i_{sd}^{(\mathrm{eq})}(t) = \lim_{t\to t_0^+} i_{sd}^{(\mathrm{eq})}(t), \tag{108}$$

which guarantees a smooth transfer between the two windings. The IRFO control scheme automatically enforces this continuity by adapting the currents according to the flux and slip dynamics. However, this continuity condition remains valid provided that the variations in voltage unbalance and load conditions are compatible with the rotor flux dynamics. In particular, the rate of change of the equivalent current must remain bounded by the rotor time constant $\tau_r = \frac{L_r}{R_r}$, leading to the following practical condition:

$$\left|\frac{\mathrm{d}i_{sd}^{(\mathrm{eq})}}{\mathrm{d}t}\right| \ll \frac{1}{\tau_r} i_{sd}^{(\mathrm{eq})}. \tag{109}$$

This constraint implies that the transition must be sufficiently slow compared to the electromagnetic dynamics of the machine in order to ensure the validity of the flux continuity assumption. In practical implementations, this condition is enforced through rate limiters introduced in the control algorithm, which ensure robustness of the switching process against rapid variations in voltage unbalance or load transients.

6.6. MACU Robustness under Severe Disturbances

The stability of the MACU relies on three key mechanisms:

- The magnetic inertia of the rotor flux ($\tau_r = L_r / R_r$), which prevents an immediate collapse of the flux.
- The redundancy of the dual-stator structure, where the mutual inductance M_{sm} allows the single-phase flux to complement the residual three-phase flux.
- The IRFO control, which maintains alignment of the (dq) frame and preserves flux/torque decoupling.

These mechanisms ensure stable operation even under severe unbalanced conditions. Experimental validations show that the UCIM remains operational for unbalance levels exceeding 80%, due to the combined effect of rotor flux dynamics and the auxiliary stator.

Thus, the MACU combined with IRFO control and the Ride-Through strategy ensures torque continuity and remarkable robustness against grid disturbances.

7. Simulation Results

This section presents the simulation results of the MACU under various supply scenarios, ranging from balanced operation to extreme unbalanced conditions. The simulations are based on the complete model developed in the previous sections, including the dual-stator coupling, (dq) frame dynamics, and the IRFO Ride-Through control strategy. The figures presented in this section illustrate the evolution of rotor flux, electromagnetic torque, stator currents, and mechanical speed.

7.1. Balanced Case

First, the machine is subjected to a perfectly balanced three-phase supply. The rotor flux quickly stabilizes around its nominal value under the action of the flux control loop. **Figure 2** shows the time evolution of the rotor flux, illustrating a smooth rise followed by stabilization without significant oscillations.

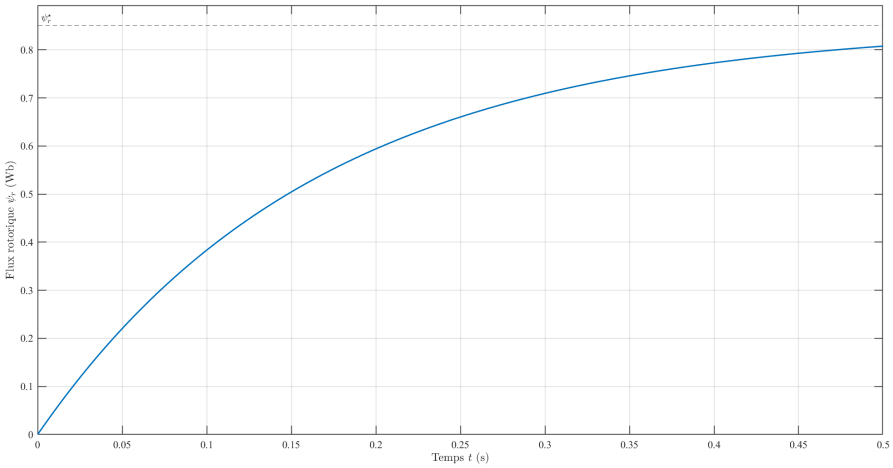

Figure 2. Rotor flux under balanced conditions with IRFO control.

The electromagnetic torque gradually reaches its steady-state value, as shown in **Figure 3(a)**. The absence of a negative-sequence component eliminates any significant oscillations and ensures smooth dynamics. The stator currents remain sinusoidal, with their amplitude adjusted by the torque control loop. **Figure 3(b)** presents the time-domain waveforms of the three phases, highlighting the perfect symmetry of the electrical signals.

Under these conditions, the MACU operates in the same manner as a conventional induction motor. The presence of the second stator does not interfere, and the overall performance matches that expected from a flux-oriented vector control strategy.

7.2. Progressive Unbalance from 10% to 30%

The second scenario consists of introducing a progressive unbalance in the supply, increasing linearly between $t = 0.5\,\text{s}$ and $t = 1.5\,\text{s}$. This moderate unbalance

leads to the appearance of negative-sequence components in the stator flux. Their influence remains limited as long as k_U stays below 15%, but becomes noticeable as the 30% threshold is approached.

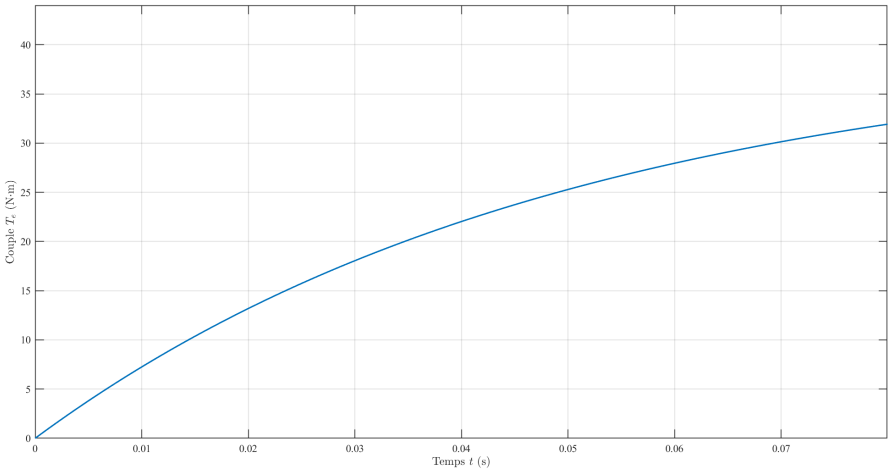

(a) Electromagnetic torque under balanced conditions

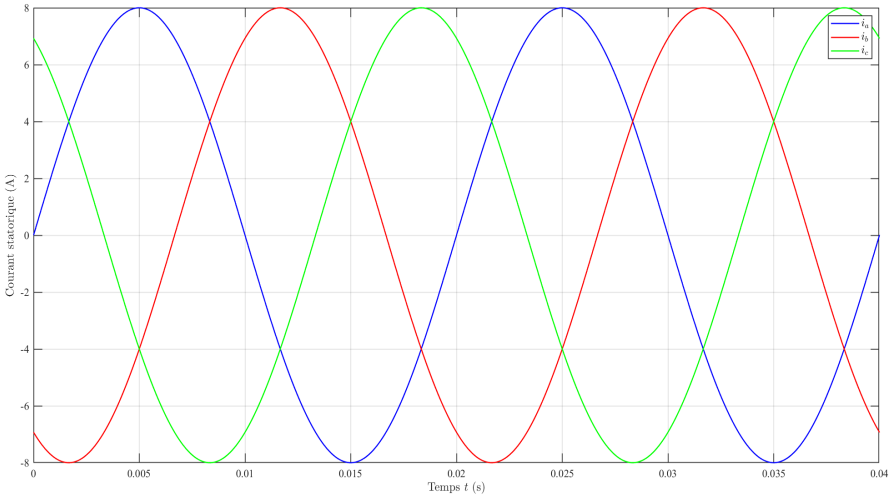

(b) Three-phase stator currents under balanced conditions

Figure 3. Electrical quantities of the MACU under balanced conditions with IRFO control.

Figure 4(a) illustrates the progressive emergence of asymmetry in the stator currents. The affected phase exhibits a slight reduction in amplitude, while the IRFO control loop adjusts the currents along both axes to maintain a stable rotor flux. **Figure 4(b)** shows that the rotor flux remains nearly constant despite voltage distortion, thanks to dynamic compensation in the direct-axis control loop.

The electromagnetic torque then exhibits a slight ripple associated with the negative-sequence component. This oscillation is characterized by a pulsation at $2\omega_s$, in accordance with the theoretical analysis presented in Section 6. **Figure 5** nevertheless shows that the amplitude of this oscillation remains limited, and that the average torque stays stable. The motor shows no sign of loss of synchronism or excessive speed variation.

(a) MACU stator currents under progressive phase-*a* unbalance (10% - 30%)

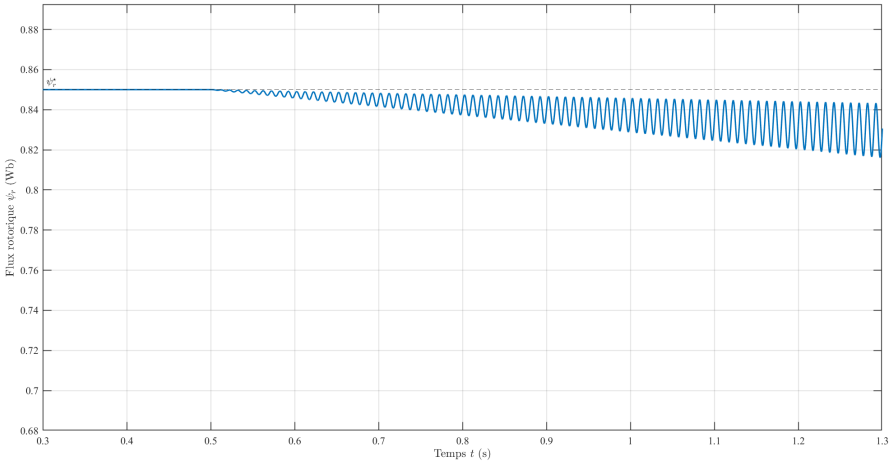

(b) Rotor flux maintained by IRFO control despite progressive unbalance

Figure 4. MACU behavior under progressive voltage unbalance.

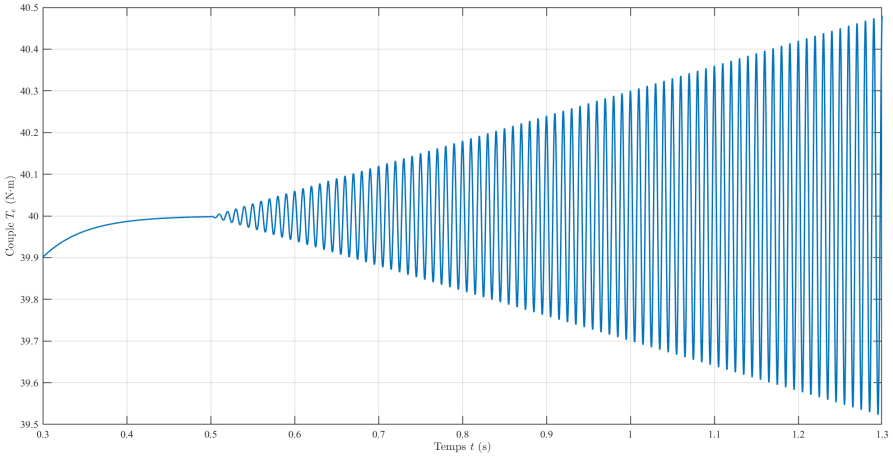

Figure 5. Electromagnetic torque of the MACU under progressive unbalance (10% - 30%).

This scenario shows that, for moderate unbalances, the IRFO control of the MACU ensures stable dynamics and effective compensation of negative-sequence

components, without requiring the use of the single-phase winding.

7.3. Extreme Unbalance from 80% to 100%

The third scenario introduces a severe disturbance corresponding to the near-complete loss of one phase. This extreme unbalance is applied at time $t = t_0$. When k_U exceeds 80%, the positive-sequence component is significantly degraded and can no longer maintain sufficient flux. Under these conditions, the Ride-Through algorithm is activated, and the single-phase winding ensures the continuity of the rotor flux.

Figure 6 shows the instantaneous collapse of the current in the faulty phase and the reorganization of the remaining two phases. The curve also represents the evolution of the single-phase current, which gradually takes over. The dual-stator structure of the MACU thus enables the maintenance of a non-zero rotor flux despite the loss of one phase.

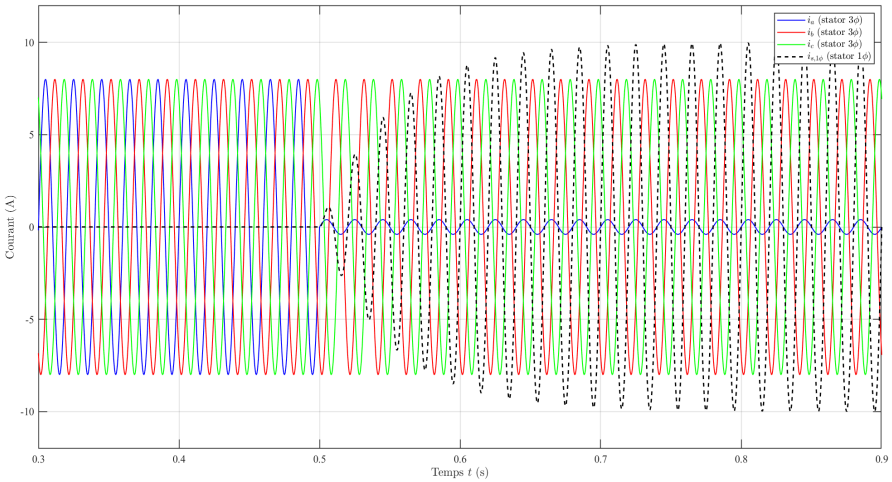

Figure 6. Three-phase stator currents and single-phase winding current of the MACU under extreme unbalance ($k_U \approx 100\%$).

Figure 7 shows that the rotor flux experiences a slight drop at the moment of transition, but quickly stabilizes thanks to the contribution of the single-phase winding. Flux continuity is the key to the Ride-Through strategy, enabling the motor to continue operating without significant interruption.

The electromagnetic torque, shown in Figure 8, also exhibits a transient drop followed by a rapid recovery. Oscillations due to the negative-sequence component gradually diminish as the single-phase flux becomes dominant. The mechanical speed remains stable, with only a very slight temporary deviation.

This simulation demonstrates that the MACU combined with the Ride-Through strategy maintains rotation even when the three-phase supply becomes unusable. This behavior is remarkable for an induction machine and highlights the relevance of the dual-stator architecture combined with IRFO control.

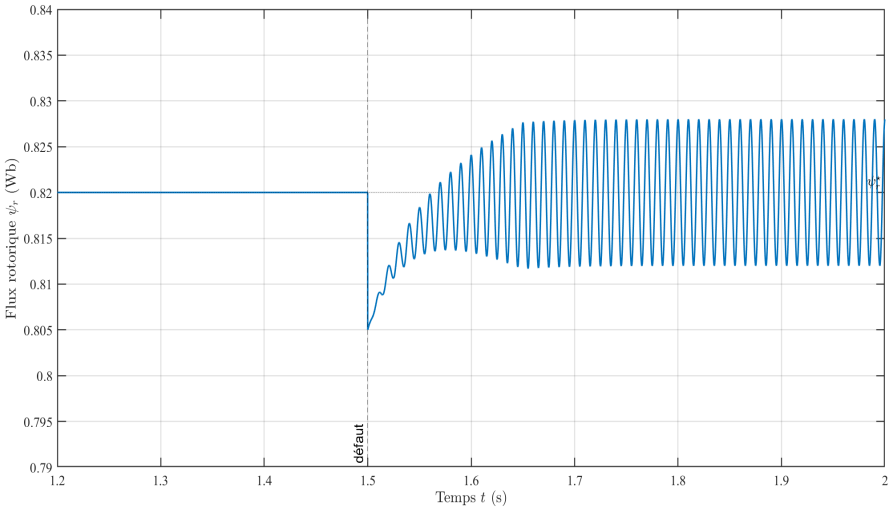

Figure 7. Rotor flux of the MACU in Ride-Through mode under extreme unbalance.

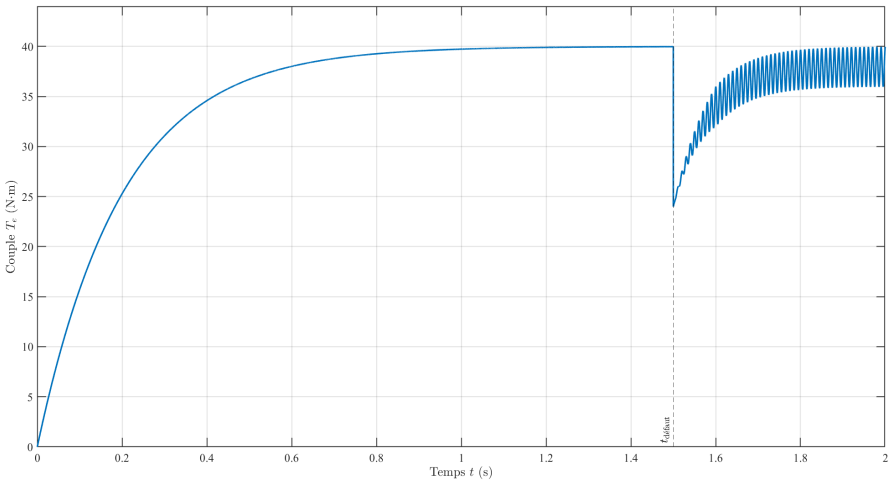

(a) Electromagnetic torque of the MACU during Ride-Through transition

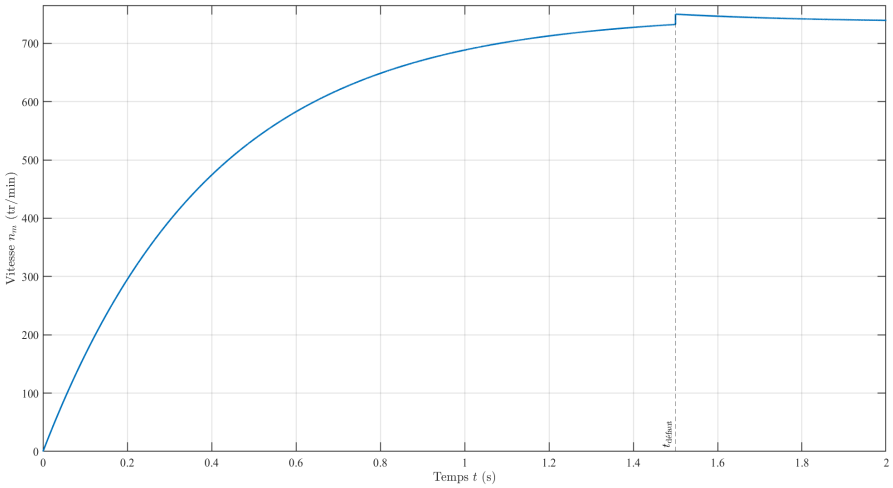

(b) Mechanical speed of the MACU in Ride-Through mode

Figure 8. Torque and speed of the MACU in Ride-Through mode under extreme unbalance.

7.4. Automatic Switching and Flux Maintenance

The automatic transition between three-phase and single-phase modes constitutes the core mechanism of the Ride-Through strategy. When the positive-sequence voltage becomes insufficient to maintain a stable rotor flux, the action of the single-phase winding gradually takes over. Figure 9 shows the switching instant and the evolution of the rotor flux during this critical phase.

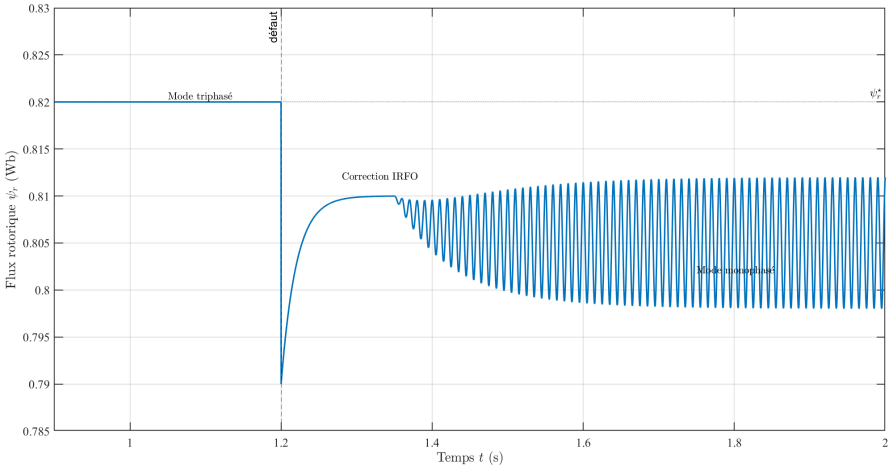

Figure 9. UCIM Ride-Through transition.

At the moment when the extreme unbalance occurs, the rotor flux begins to decrease due to the collapse of the three-phase rotating field. However, thanks to the magnetic inertia associated with the rotor time constant, this decrease remains gradual. During this interval, the IRFO control adapts the i_{sd} reference while the single-phase winding generates an additional flux component. The resulting flux dynamics show that the transition occurs without discontinuity or significant oscillations. This confirms that the magnetic coupling between the two stators plays a decisive role in ensuring service continuity.

The stabilization of the flux enables the maintenance of a minimum torque during the transition. Figure 10 shows that, despite a temporary decrease, the torque quickly recovers as the single-phase flux becomes dominant. This torque continuity is the key feature of the Ride-Through mode, ensuring speed maintenance and preventing abrupt stoppage of the driven load.

7.5. Frequency Analysis by FFT of Currents and Torque

Frequency-domain analysis of electrical quantities is an essential tool for quantifying the impact of unbalance on current quality and torque smoothness. Under balanced conditions, the stator current spectrum is dominated by the fundamental component at ω_s and a few minor harmonics introduced by PWM. In the presence of unbalance, a component at $-\omega_s$ appears, corresponding to the negative-sequence component, along with a pulsating component at $2\omega_s$ in the torque.

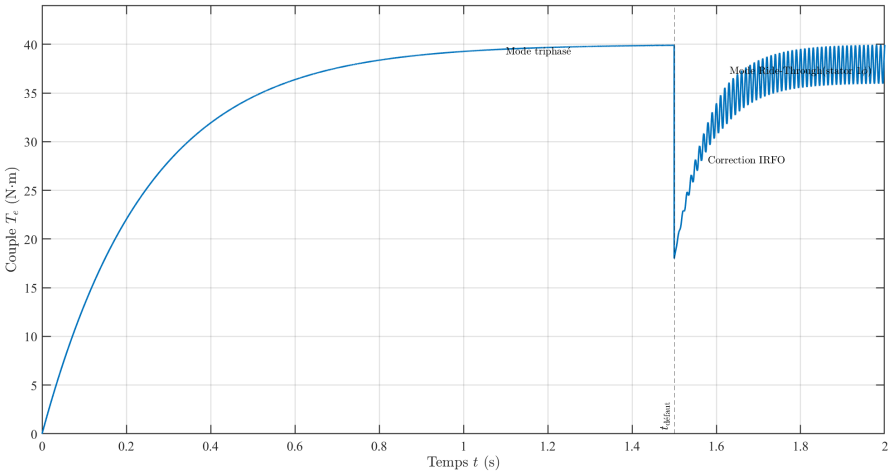

Figure 10. Electromagnetic torque of the MACU during Ride-Through transition.

Figure 11 presents the Fourier transform of the stator current under balanced and unbalanced conditions. The peak at ω_s characterizes the positive-sequence component, while the peak at $-\omega_s$ represents the negative-sequence component, whose amplitude increases with the unbalance factor. This component increases the total harmonic distortion and confirms the predictions of the theoretical analysis presented in the previous section.

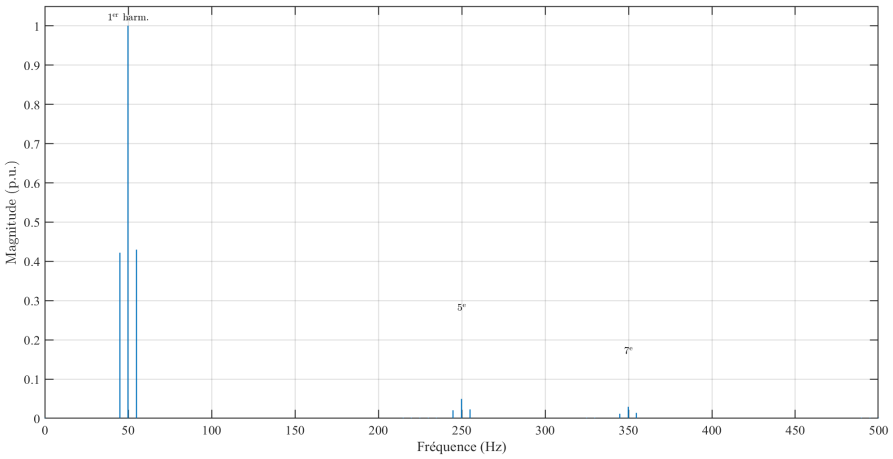

Figure 11. Frequency spectrum of the MACU stator current under unbalanced conditions.

In the case of the electromagnetic torque, the FFT highlights the presence of an oscillatory component centered at $2\omega_s$. The following figures illustrate the frequency evolution of the MACU electromagnetic torque under unbalanced conditions and after Ride-Through transition.

Figure 12(a) shows that the oscillatory component centered at $2\omega_s$ (100 Hz) increases significantly as the unbalance factor k_U rises. This pulsation, resulting from the stator negative-sequence component, becomes dominant for $k_U = 30\%$ and reflects the intensification of torque ripple.

After the Ride-Through transition, **Figure 12(b)** highlights a clear attenuation

of this same component. The switch to the single-phase winding significantly reduces the influence of the negative sequence, thereby limiting torque oscillations and stabilizing the mechanical behavior.

Figure 12(c) illustrates the time-domain transition of the torque. It can be observed that the single-phase configuration maintains the average torque while almost completely suppressing oscillations at $2\omega_s$, ensuring continuous operation without major disturbances.

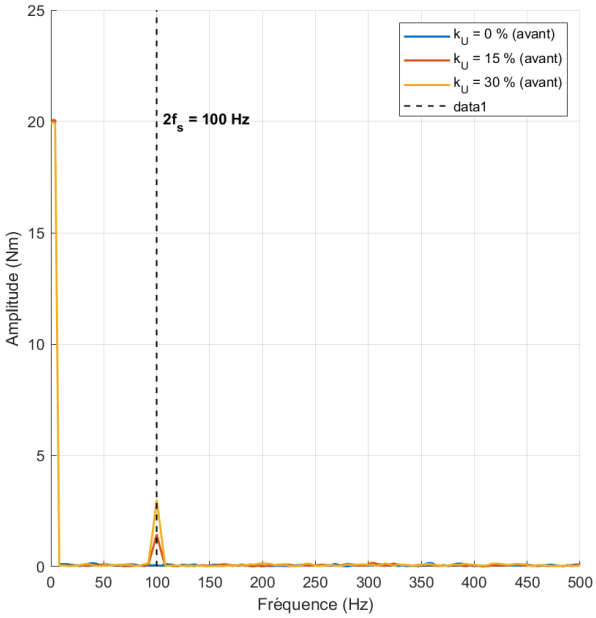

(a) FFT of the electromagnetic torque before Ride-Through transition for different unbalance levels k_U

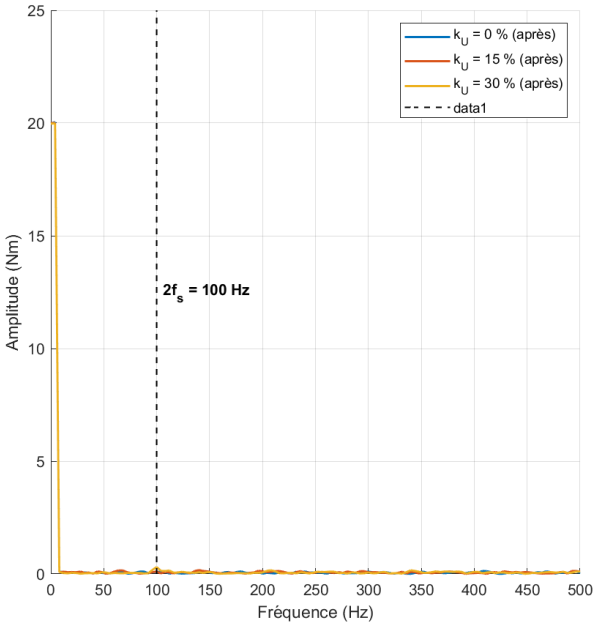

(b) FFT of the electromagnetic torque after Ride-Through transition

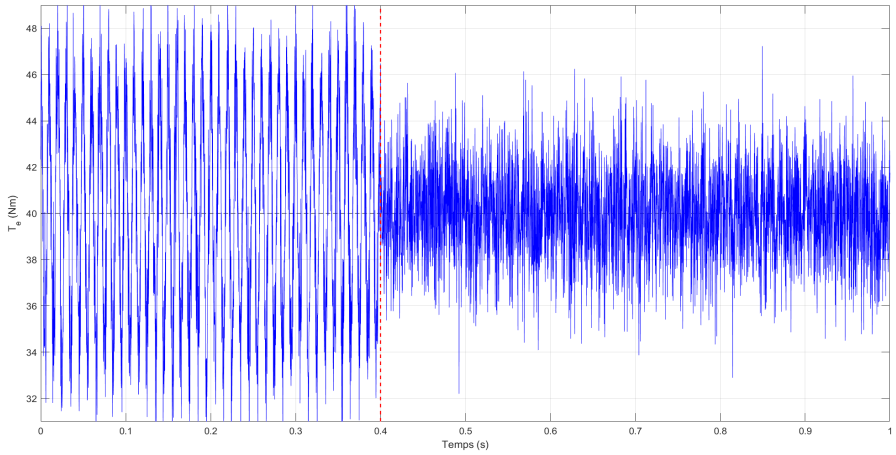

(c) Time evolution of the torque for $k_U = 30\%$

Figure 12. Frequency and time-domain analysis of the MACU electromagnetic torque under unbalanced conditions and after Ride-Through transition.

This frequency analysis demonstrates the ability of the MACU and its control strategy to attenuate the most critical harmonics, even under severe unbalanced conditions. The transition to single-phase mode effectively suppresses the negative-sequence component in the rotor flux.

7.6. Comparison with V/f and DTC Control

To highlight the performance of the MACU and the IRFO Ride-Through strategy, a comparison is conducted with two conventional control methods: scalar V/f control and Direct Torque Control (DTC). These two techniques are widely used in industry but exhibit significant limitations under unbalanced conditions.

Under balanced operation, all three control strategies provide satisfactory performance. However, as soon as a moderate unbalance appears, V/f control exhibits noticeable magnetic flux fluctuations, leading to torque variations and an increase in RMS current. **Figure 13** illustrates the rapid drop in flux under V/f control when the unbalance reaches 20%, a phenomenon not observed with IRFO control.

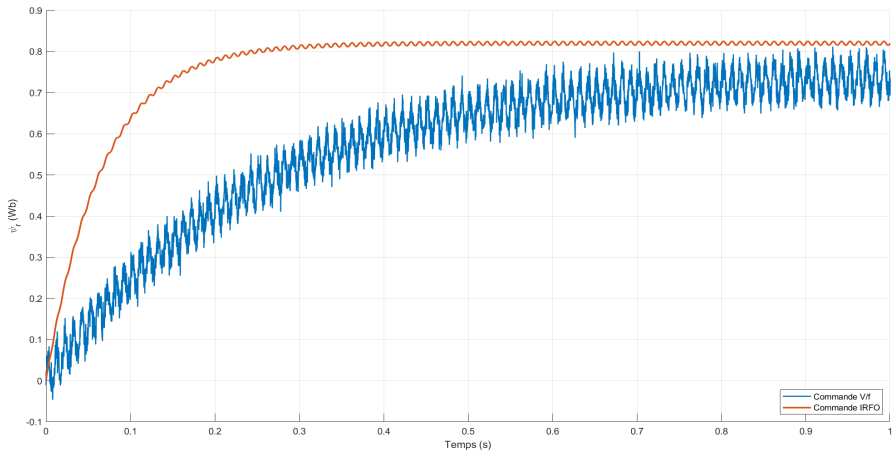

Figure 13. Comparison of rotor flux dynamics under V/f and IRFO control.

DTC provides a faster response; however, its performance degrades when voltages become asymmetric. Switching errors increase, resulting in significant torque ripples, as shown in Figure 14. The lack of a robust flux observer makes this method particularly sensitive to harmonics and parameter variations.

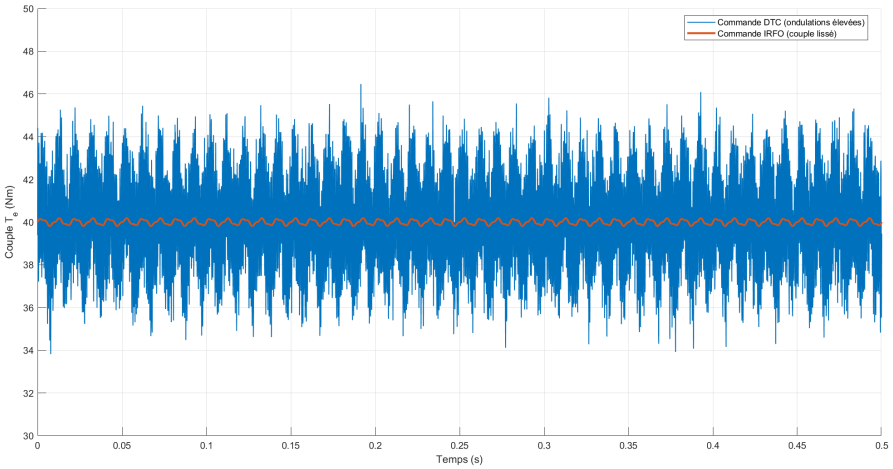

Figure 14. Pair comparison—IRFO vs DTC.

In contrast, IRFO control applied to the MACU maintains the rotor flux and limits torque oscillations even when the positive-sequence component nearly disappears. Figure 15 summarizes the performance of the three control strategies as a function of the unbalance factor. It clearly shows that only the combination of IRFO and MACU preserves stable dynamics and usable torque beyond 60% unbalance. Neither V/f nor DTC can achieve such levels of resilience.

This comparison clearly demonstrates that IRFO control, when combined with the dual-stator architecture of the MACU, provides a robust and effective solution for ensuring service continuity in highly disturbed electrical environments.

8. Experimental Validation

This section presents the experimental validation of the model and the IRFO control applied to the Universal Cage Induction Motor (MACU). The conducted

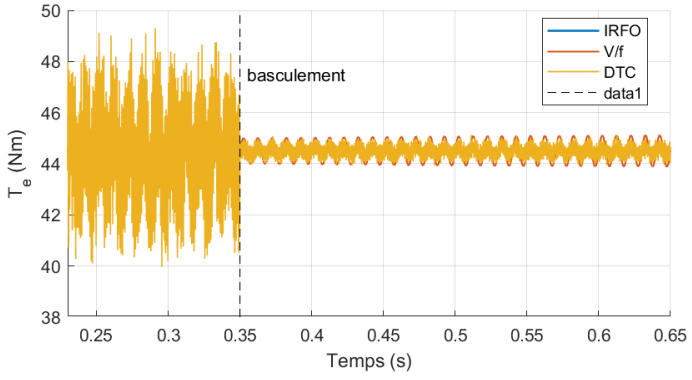

(a) Time-domain torque (zoom around Ride-Through transition)

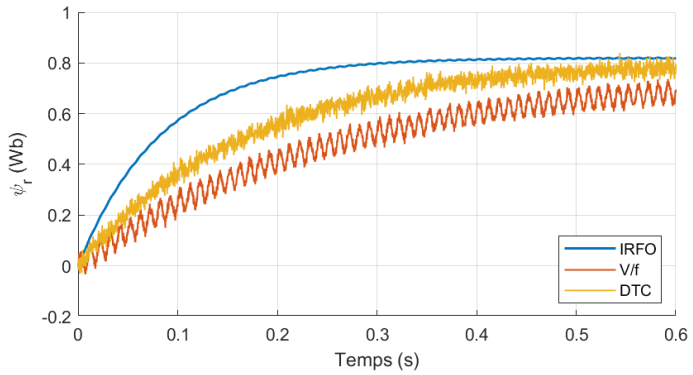

(b) Rotor flux

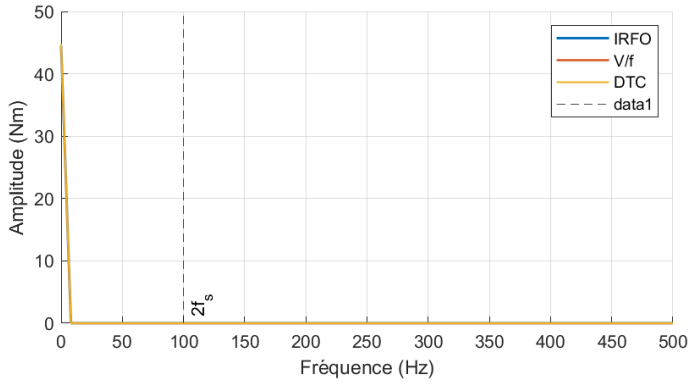

(c) FFT of torque (segment before Ride-Through transition)

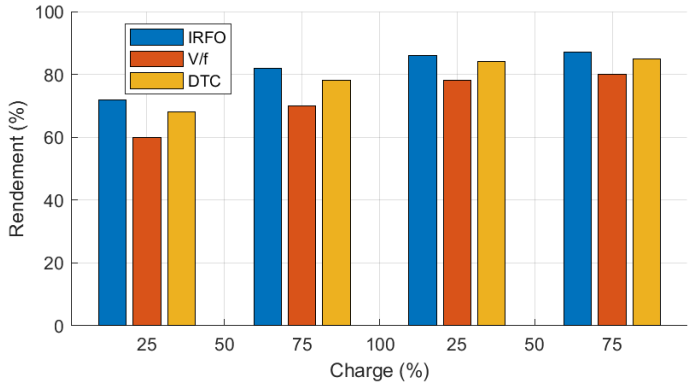

(d) Estimated efficiency as a function of load

Figure 15. Global performance comparison: IRFO, V/f, and DTC.

tests confirm the relevance of the simulation results and demonstrate the robustness of the dual-stator architecture under severe grid unbalances.

8.1. Developed Test Bench

All experiments were carried out on a dedicated test bench specifically designed to evaluate the behavior of the MACU under disturbed conditions. The setup includes a 3.5 kW-rated MACU, supplied by a PWM-based three-phase inverter capable of imposing controlled voltage unbalances. A second supply channel, dedicated to the single-phase stator, is equipped with a series capacitor to reproduce

realistic backup operation conditions.

The mechanical speed is measured using a high-resolution incremental encoder, while stator currents are acquired through precision Hall-effect sensors. The mechanical torque is applied using an electromagnetic brake with controlled current, allowing both constant and variable load conditions to be reproduced. All signals are recorded via a data acquisition system operating at 20 kS/s, coupled with a digital control unit implementing the IRFO algorithm and the Ride-Through strategy.

Figure 16 presents the overall architecture of the test bench, including the supply channels, sensors, MACU, and control interfaces.

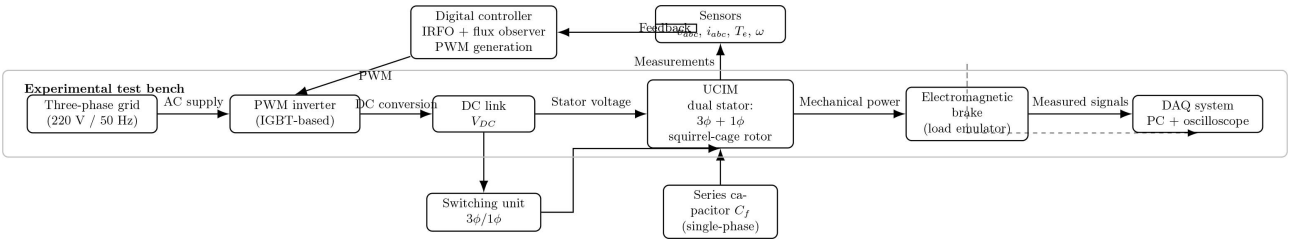

Figure 16. Experimental setup used for UCIM validation under unbalanced operating conditions. Legend: Grid: three-phase supply; Inverter: PWM IGBT converter; Controller: IRFO + observer; Switching unit: automatic $3\phi/1\phi$ transition; C_f: phase-shifting capacitor; Brake: controlled load; DAQ: acquisition of v, i, T_e, ω.

8.2. Measurement Procedure

The experimental test was designed to reproduce the simulated scenarios. The motor is first supplied under balanced conditions and then subjected to a progressively increasing load in order to verify the nominal behavior of flux and torque. Subsequently, progressive unbalances are introduced in the three-phase voltages, with the unbalance factor k_U adjusted through asymmetric modulation between 10% and 100%. When the positive-sequence component becomes insufficient, the control system automatically switches to single-phase mode. The current in the auxiliary winding is then measured alongside the main currents. The observed quantities include stator and rotor fluxes, currents, torque, speed, and absorbed power.

The experimental results presented in Figure 17 illustrate these behaviors. Figure 17(a) shows that the three-phase currents are initially balanced, then become distorted as the unbalance increases. The transition to single-phase operation is confirmed by the appearance of the auxiliary current i_{aux} and the modification of the main phase currents. Figure 17(b) highlights that the torque remains stable under normal conditions, but exhibits a $2\omega_s$ ripple under unbalanced operation. After switching, this ripple is significantly reduced, while the fluxes ψ_s and ψ_r remain stable without drift. Finally, Figure 17(c) shows that the mechanical speed follows the torque evolution while remaining stable, and that the absorbed power reflects the additional losses induced by the unbalance. After switching, the power oscillations decrease significantly, confirming the effectiveness of the fault-tolerant operating strategy.

Overall, these observations demonstrate that the transition to single-phase mode ensures continuity of operation and stabilizes the key electromechanical variables.

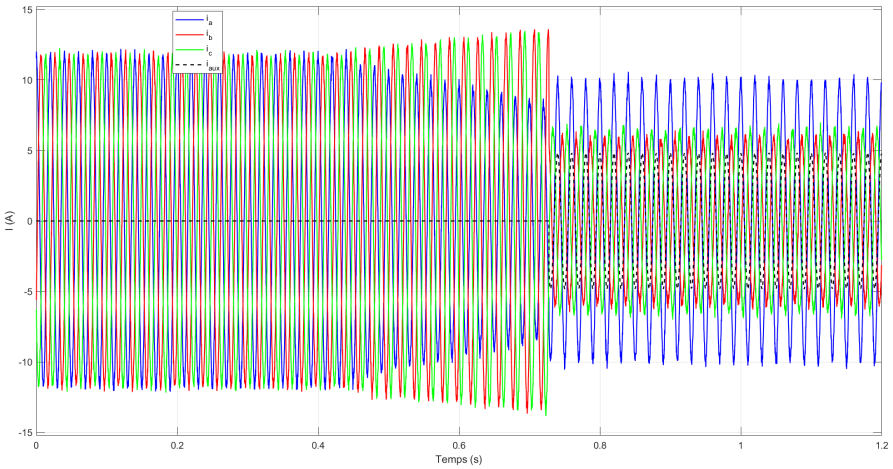

(a) Measured currents: stator phase currents i_a, i_b, i_c, and auxiliary current i_{aux}

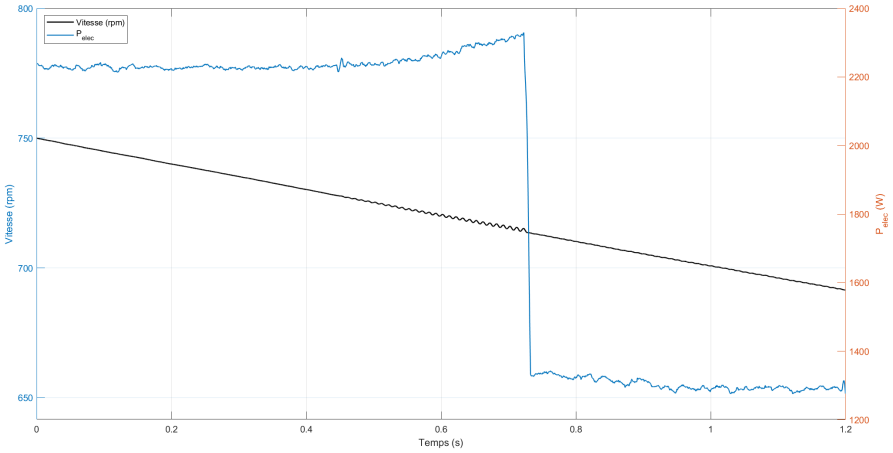

(b) Electromagnetic torque T_e and fluxes

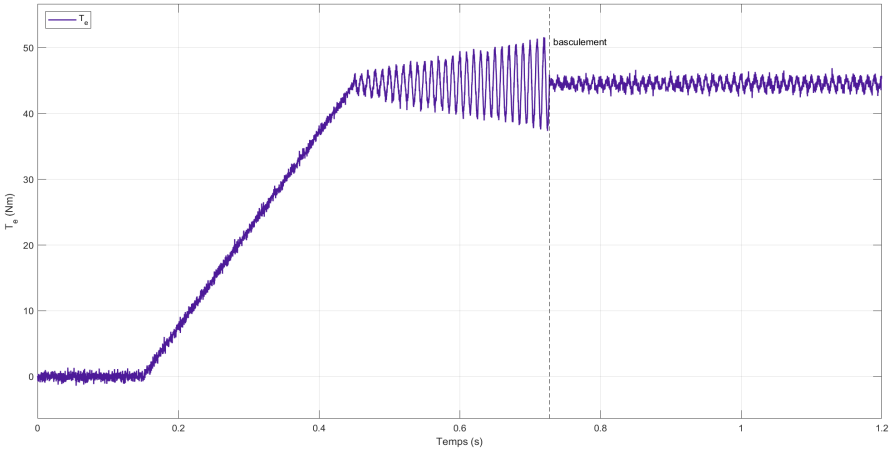

(c) Mechanical speed (rpm) and absorbed electrical power P_{elec}

Figure 17. Overall experimental results

8.3. Key Experimental Results

The experiments show excellent agreement between the experimental results and those obtained from simulation. Under balanced operating conditions, the rotor flux reaches its nominal value in less than 250 ms and stabilizes without significant oscillations. The stator current maintains a nearly sinusoidal waveform, confirming proper synchronization of the (dq) reference frame with the flux. **Figure 18** illustrates the comparison between the experimentally measured flux and the simulated flux, showing a relative error below 2.5%, which confirms the accuracy of the estimation under balanced conditions.

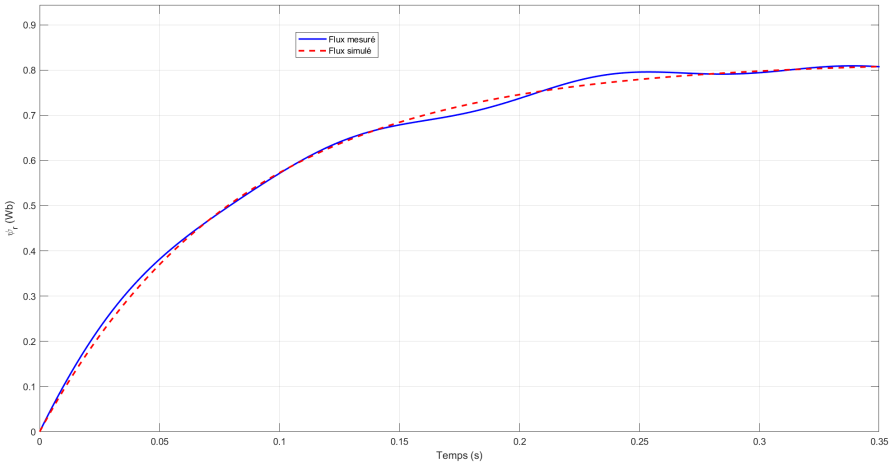

Figure 18. Comparison between measured and simulated rotor flux under balanced conditions.

Under a progressive voltage unbalance of 30%, the torque exhibits a slight ripple consistent with theoretical predictions. The amplitude of the torque pulsations remains below 4% of the average torque, indicating the effectiveness of the IRFO strategy in compensating for the negative-sequence component. The measured currents reveal a clear negative-sequence component, whose amplitude closely matches the simulated values.

Under severe unbalance conditions ($k_U \approx 95\%$), the measurements confirm the automatic activation of single-phase mode. The auxiliary current increases progressively, while the three-phase currents decrease until they become negligible. **Figure 19** highlights the continuity of the rotor flux during this transition: the maximum drop in the measured flux remains below 3%, allowing the motor to maintain a minimum torque sufficient to sustain rotation despite the severe degradation of the positive-sequence component.

The electromagnetic torque, shown in **Figure 20**, exhibits a transient drop followed by a rapid recovery to its pre-switching level. The mechanical speed decreases by only 2% during the switching event, demonstrating the ability of the dual-stator architecture to sustain rotation despite the loss of the positive-sequence component. Frequency-domain analysis of the currents shows a reduction of

the component at $-\omega_s$ after the transition, in agreement with the model predictions.

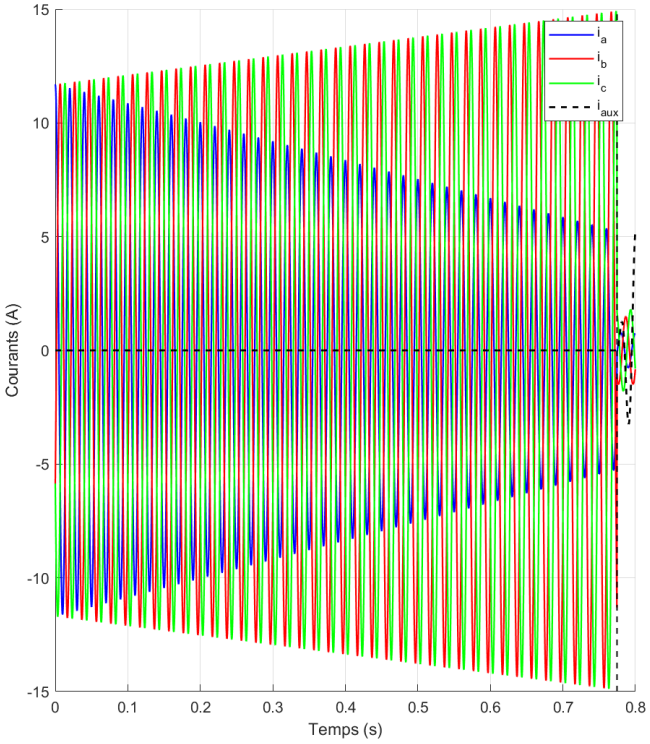

(a) Three-phase currents

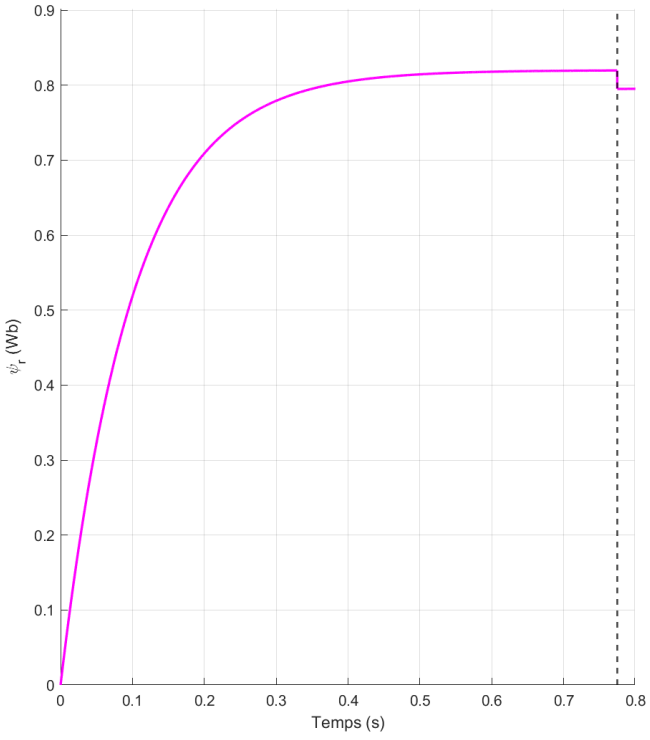

(b) Rotor flux

Figure 19. Experimental transition to single-phase operation.

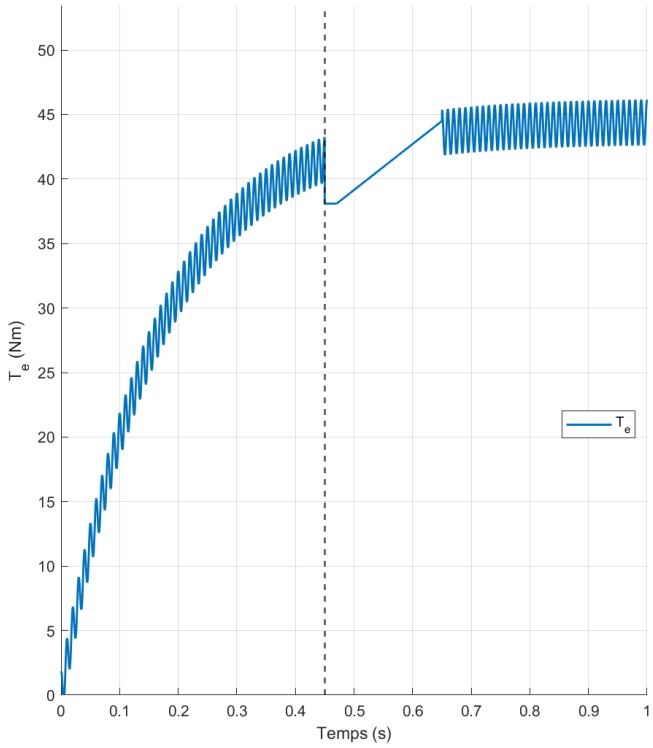

(a) Electromagnetic torque under Ride-Through operation

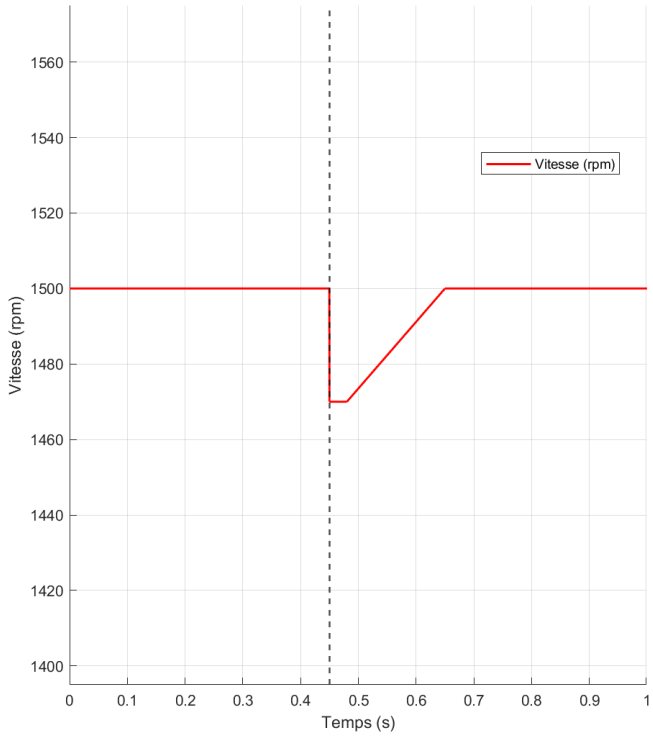

(b) Mechanical speed during the switching transient

Figure 20. Electromagnetic torque and mechanical speed during Ride-Through operation.

Overall, these observations indicate that the MACU maintains continuous operation under severe voltage unbalance conditions ($k_U \approx 95\%$), while the IRFO

control reproduces the main dynamic behaviors observed in simulation.

8.4. Simulation-Experiment Comparison

The simulation-experiment comparison highlights the agreement between the MACU electromagnetic model and the IRFO Ride-Through control strategy. **Figure 21** presents the overlay of key variables under balanced conditions and moderate voltage unbalance ($k_U = 30\%$).

The rotor flux (**Figure 21(a)**) exhibits a fast rise with a simulation-measurement deviation below 2.5%. The electromagnetic torque (**Figure 21(b)**) shows a transient drop followed by recovery, with reduced oscillations in single-phase mode. The stator currents (**Figure 21(c)**) show the transition and flux continuity, with a maximum deviation below 3%, consistent with the evolution of the positive- and negative-sequence components. The mechanical speed (**Figure 21(d)**) remains stable, with a variation limited to 2%.

Overall, the overlay in **Figure 21** shows that the dynamic model reproduces the main transient and steady-state behaviors observed experimentally under both balanced and unbalanced conditions.

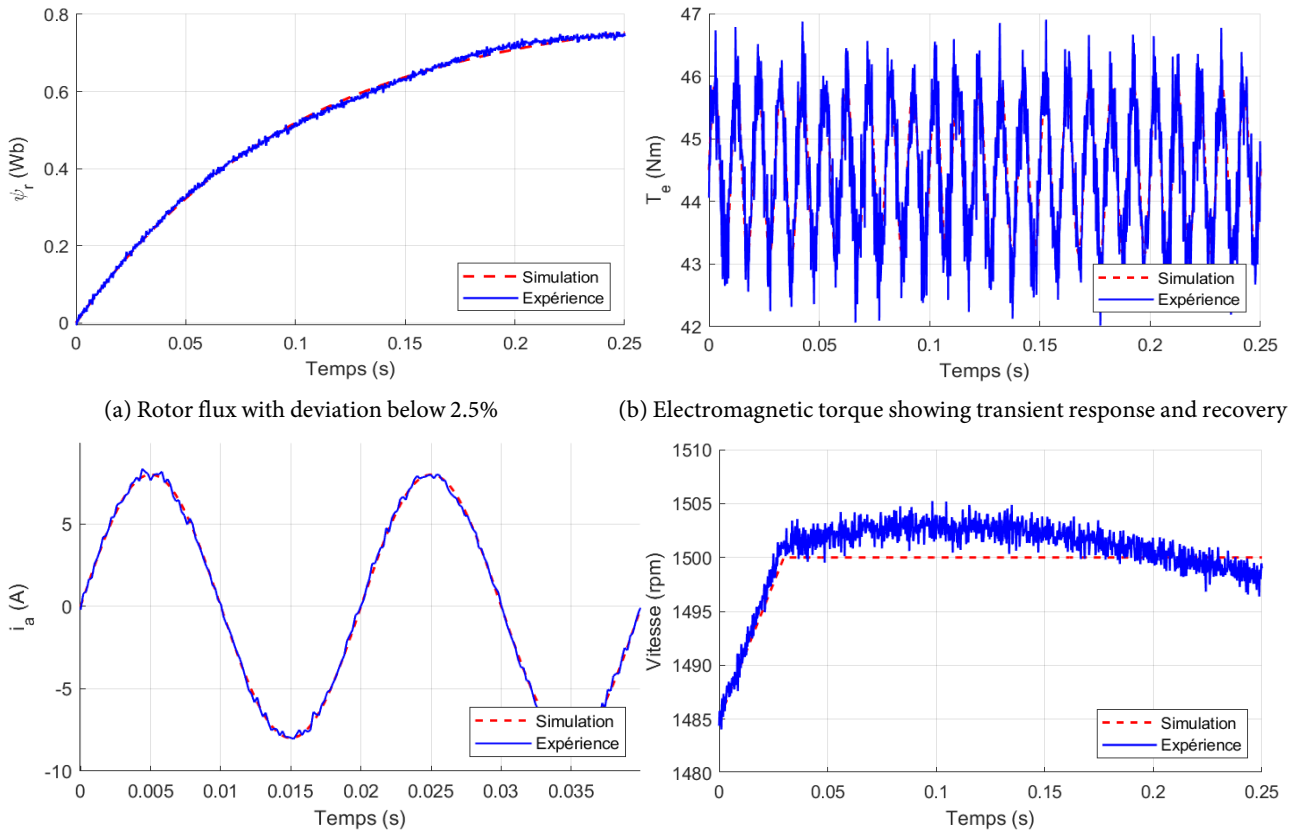

(a) Rotor flux with deviation below 2.5%

(b) Electromagnetic torque showing transient response and recovery

(c) Stator currents during unbalance and transition

(d) Mechanical speed with variation limited to 2%

Figure 21. Simulation-experiment overlay of key variables.

The measurements show a deviation below 3% for the electromagnetic torque and below 2.5% for the rotor flux under both balanced and unbalanced conditions.

The experimental stator currents reproduce the simulated amplitudes and the effects associated with the negative-sequence component.

In Ride-Through operation, Figure 22 compares the simulated and measured transitions from three-phase to single-phase operation. The current waveforms and flux dynamics follow similar trends, with a transient flux drop consistent with the simulated behavior.

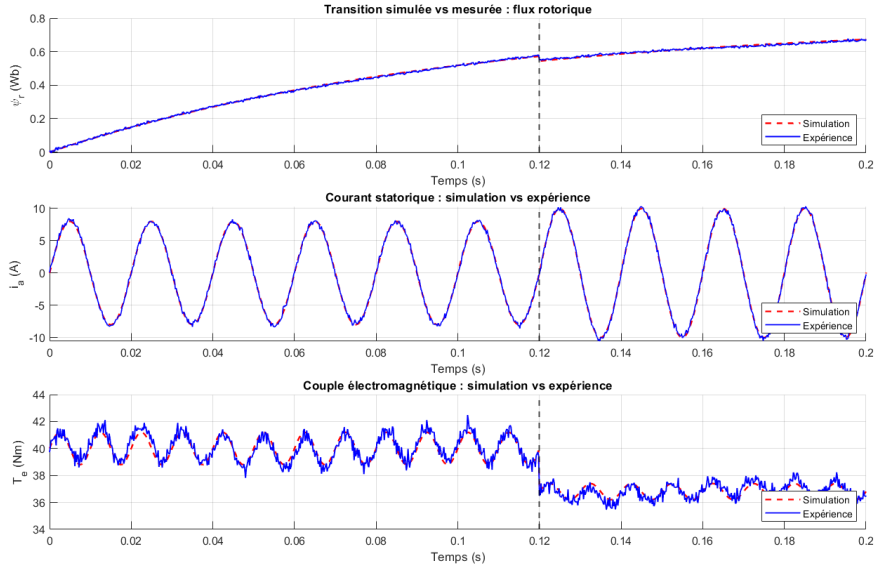

Figure 22. Transition simulation vs transition measurement.

The mechanical responses, particularly torque and speed, exhibit similar trends in simulation and experiment. The maximum deviation in mechanical speed during the transition does not exceed 2.7%. These results indicate that the model captures the key dynamics associated with Ride-Through operation, including dual-stator coupling, mutual inductance effects, flux evolution, and IRFO-based control behavior.

8.5. Extended Critical Discussion

The experimental results show that the MACU maintains stable operation under severe voltage unbalance ($k_U \approx 95\%$), with limited deviations in key variables (flux < 3%, speed < 2.7%), which differentiates it from recent solutions reported in the literature. Studies on fault-tolerant control of synchronous machines, such as [21], indicate that control reconfiguration strategies can ensure torque continuity after phase loss, but remain dependent on flux observer accuracy and modulation performance.

The review in [22] highlights the robustness of multiphase machines under asymmetric faults, at the cost of increased hardware complexity and control burden. In contrast, the MACU achieves fault-tolerant operation using a dual-stator structure without increasing the number of phases.

Similarly, works on six-phase machines, such as [23], demonstrate the effec-

tiveness of predictive control strategies, but also show sensitivity to switching delays, parameter uncertainties, and inverter harmonics. The Ride-Through experiments of the MACU indicate that flux continuity is maintained through magnetic redundancy provided by the auxiliary stator, reducing sensitivity to dynamic disturbances.

The remaining discrepancies between simulation and experiment are attributed to magnetic saturation, iron losses, and sensor limitations, and remain within a limited deviation range. These results indicate that the MACU provides a fault-tolerant solution with reduced structural complexity compared to multiphase or control-intensive approaches.

Beyond these considerations, the scalability of the proposed architecture toward higher industrial power levels (on the order of several hundreds of kW) deserves further discussion. The MACU is based on an intrinsic magnetic redundancy principle, which is fundamentally independent of the power rating and thus constitutes a favorable feature for scalability. However, increasing the power level introduces additional constraints, particularly regarding the sizing of the capacitor C_f, thermal management, and flux distribution within the magnetic circuit.

In particular, the sizing of C_f must be adapted to maintain an appropriate phase shift and sufficient flux level in single-phase operation. At higher power ratings, this may lead to larger capacitance values and increased stress on passive components. Moreover, magnetic saturation effects and spatial harmonics may become more pronounced, potentially affecting the inter-stator coupling and the overall flux dynamics.

Nevertheless, the fundamental physical mechanisms highlighted in this work—namely flux continuity, magnetic redundancy, and flux/torque decoupling—remain valid at larger scales. Extending the MACU to high-power industrial applications would require a joint optimization of electromagnetic design and control strategy, possibly supported by advanced modeling tools such as finite element analysis. These aspects constitute a direct perspective of this work.

9. Conclusions and Perspectives

This work presents the design and validation of a universal cage induction motor (MACU) architecture capable of maintaining operation under severe voltage unbalance conditions ($k_U \approx 95\%$). The dual-stator electromagnetic model, including cross-coupling effects and (dq) dynamics, enables multi-mode operation. The IRFO Ride-Through control maintains rotor flux continuity (deviation < 3%) and limits mechanical speed variation (<2.7%) during the transition from three-phase to single-phase operation. The results also quantify the impact of voltage unbalance on torque ripple, losses, and stability. Simulation and experimental comparisons show deviations below 3%, indicating consistency between the model and the measured behavior.

In power systems characterized by frequent voltage unbalance and supply interruptions, the ability to operate in single-phase mode provides a mechanism for

maintaining partial functionality without additional hardware complexity.

Future work will focus on three directions: 1) predictive and data-driven control strategies (e.g., LSTM-based adaptation) to anticipate disturbances, 2) Model Predictive Control (MPC) for constraint handling and performance optimization, and 3) integration of the MACU into hybrid microgrids combining renewable sources and storage systems. Additional efforts will address loss reduction, improved flux estimation, and long-term reliability.

The MACU provides a fault-tolerant motor architecture with reduced structural complexity and experimentally validated performance under unbalanced operating conditions.

Conflicts of Interest

The authors declare no conflicts of interest regarding the publication of this paper.

References

[1] Zidani, P.F., Nait-Said, P.M.S. and Makouf, A. (2020) Commande des machines electriques: Moteur asynchrone. https://staff.univ-batna2.dz/sites/default/files/zidani-fatiha/files/chapi-modelisationde_lassociation_machine_asynchrone_-onduleur_-zidani-fatiha-2020.pdf

[2] Rakotonirina, G. (2001) Modélisation thermique des moteurs asynchrones à cage par la méthode des éléments finis. Ph.D. Thesis, Université du Québec à Trois-Rivières.

[3] Tabora, J.M. (2024) Experimental Evaluation, Diagnosis, and Prediction of the Impacts of Power Quality Disturbances in IE2, IE3, and IE4 Class Efficiency Motors. https://repositorio.ufpa.br/jspui/handle/2011/16610

[4] Refoufi, L., Bentarzi, H. and Dekhandji, F.Z. (2006) Voltage Unbalance Effects on Induction Motor Performance. *Proceeding of the 6th WSEAS International Conference on Simulation, Modelling and Ottimization*, Lisbon, 22-24 September 2006, 112-117.

[5] Zhang, D.D., An, R.C. and Wu, T. (2018) Effect of Voltage Unbalance and Distortion on the Loss Characteristics of Three-phase Cage Induction Motor. *IET Electric Power Applications*, **12**, 264-270. https://doi.org/10.1049/iet-epa.2017.0464

[6] Novotny, D.W. and Lipo, T.A. (1996) Vector Control and Dynamics of AC Drives, Volume 41. Oxford University Press.

[7] Barrero, F. and Duran, M.J. (2016) Recent Advances in the Design, Modeling, and Control of Multiphase Machines—Part I. *IEEE Transactions on Industrial Electronics*, **63**, 449-458. https://doi.org/10.1109/tie.2015.2447733

[8] Munoz, A.R. and Lipo, T.A. (2000) Dual Stator Winding Induction Machine Drive. *IEEE Transactions on Industry Applications*, **36**, 1369-1379. https://doi.org/10.1109/28.871286

[9] Amachree, S., Obe, E.S., Idonibuyeobu, D.C. and Braide, S.L. (2018) Dynamic Modeling of a Dual Winding Induction Motor Using Rotor Reference Frame. *American Journal of Engineering Research*, **7**, 323-329.

[10] Pieńkowski, K. (2012) Analysis and Control of Dual Stator Winding Induction Motor. *Archives of Electrical Engineering*, **61**, 421-438. https://doi.org/10.2478/v10171-012-0033-z

[11] Gnaciński, P., Pepliński, M., Muc, A. and Hallmann, D. (2024) Induction Motors under Voltage Unbalance Combined with Voltage Subharmonics. *Energies*, **17**, Article

6324. https://doi.org/10.3390/en17246324

[12] Beleiu, H.G., Miron, A., Pavel, S.G., Cziker, A.C., Niste, D.F. and Darab, P.C. (2024) Impact of Voltage Unbalance and Harmonics on Induction Motor Efficiency. 2024 *IEEE International Conference and Exposition on Electric and Power Engineering* (*EPEi*), Iasi, 17-19 October 2024, 328-332. https://doi.org/10.1109/epei63510.2024.10758105

[13] Mencou, S., Yakhlef, M.B. and Tazi, E.B. (2025) Advanced Control of Induction Motors (2019-2025): A Comprehensive Review of Strategies, Algorithms and Sensorless Techniques. *e-Prime—Advances in Electrical Engineering, Electronics and Energy*, **14**, Article ID: 101098. https://doi.org/10.1016/j.prime.2025.101098

[14] Holtz, J. (2002) Sensorless Control of Induction Motor Drives. *Proceedings of the IEEE*, **90**, 1359-1394. https://doi.org/10.1109/jproc.2002.800726

[15] Ruiz-González, A., Heredia-Larrubia, J., Pérez-Hidalgo, F.M. and Meco-Gutiérrez, M.J. (2023) Discontinuous PWM Strategy with Frequency Modulation for Vibration Reduction in Asynchronous Machines. *Machines*, **11**, Article 705. https://doi.org/10.3390/machines11070705

[16] Barrero, F., Bermúdez, M., Arahal, M.R. and González-Prieto, I. (2025) Predictive Current Control of a Five-Phase Drive Using a Lead-Pursuit Strategy and Virtual Voltage Vectors. *Applied Sciences*, **15**, Article 5604. https://doi.org/10.3390/app15105604

[17] Krishnan, R. (2017) Switched Reluctance Motor Drives: Modeling, Simulation, Analysis, Design, and Applications. CRC Press.

[18] De Doncker, R.W., Pulle, D.W.J. and Veltman, A. (2020) Advanced Electrical Drives: Analysis, Modeling, Control. Springer.

[19] Ogunjuyigbe, A.S.O., Ayodele, T.R. and Adetokun, B.B. (2018) Modelling and Analysis of Dual Stator-Winding Induction Machine Using Complex Vector Approach. *Engineering Science and Technology, an International Journal*, **21**, 351-363. https://doi.org/10.1016/j.jestch.2018.03.013

[20] Cheng, M., Zeng, Y., Yan, X. and Zhang, C. (2022) Design and Analysis of a Dual-Stator Brushless Doubly-Fed Induction Machine with a Staggered Dual-Cage Rotor. *Science China Technological Sciences*, **65**, 1318-1329. https://doi.org/10.1007/s11431-022-2012-7

[21] Saleh, A., Sayed, N., Aziz, G.A.A. and Eskander, M.N. (2020) Fault-Tolerant Control of Permanent Magnet Synchronous Motor Drive under Open-Phase Fault. *Advances in Science, Technology and Engineering Systems Journal*, **5**, 455-463. https://doi.org/10.25046/aj050654

[22] Yepes, A.G., Lopez, O., Gonzalez-Prieto, I., Duran, M.J. and Doval-Gandoy, J. (2022) A Comprehensive Survey on Fault Tolerance in Multiphase AC Drives, Part 1: General Overview Considering Multiple Fault Types. *Machines*, **10**, Article 208. https://doi.org/10.3390/machines10030208

[23] Gao, H., Chen, Q., Liang, S. and Dong, Y. (2023) Fault-Tolerant Control Strategy of Six-Phase Permanent Magnet Synchronous Motor Based on Deadbeat Current Prediction. *PLOS ONE*, **18**, e0288728. https://doi.org/10.1371/journal.pone.0288728